

Oceanic Transform Earthquakes With Unusual Mechanisms or Locations: Relation to Fault Geometry and State of Stress in the Adjacent Lithosphere

CECILY J. WOLFE, ERIC A. BERGMAN,¹ AND SEAN C. SOLOMON²

Department of Earth, Atmospheric, and Planetary Sciences, Massachusetts Institute of Technology, Cambridge

On oceanic transforms, most earthquakes are expected to occur on the principal transform displacement zone (PTDZ) and to have strike-slip mechanisms consistent with transform-parallel motion. We conducted a search for transform earthquakes departing from this pattern on the basis of source mechanisms and locations taken from the Harvard centroid moment tensor catalogue and the bulletin of the International Seismological Centre, respectively. Events with unusual mechanisms occur on several transforms. We have determined the source mechanisms and centroid depths of 10 such earthquakes on the St. Paul's, Marathon, Owen, Heezen, Tharp, Menard, and Rivera transforms from inversions of long-period body waveforms. Relative locations of earthquakes along these transforms have been determined with a multiple-event relocation technique. Much of the anomalous earthquake activity on oceanic transforms is associated with complexities in the geometry of the PTDZ or the presence of large structural features that may influence slip on the fault. Reverse-faulting earthquakes occur at a compressional bend in the Owen transform in the area of Mount Error and at the St. Paul's transform near St. Peter's and St. Paul's Rocks. A normal-faulting earthquake on the Heezen transform is located at the edge of a pull-apart basin marking an extensional offset of the fault. Normal-faulting earthquakes along the Tharp, Menard, and Rivera transforms may also be related to extensional offsets. Some events with unusual mechanisms occur outside of the transform fault zone, however, and do not appear to be related to fault zone geometry. For instance, earthquakes with mechanisms indicating reverse-faulting on ridge-parallel fault planes are located near the ridge-transform intersections of the St. Paul's and the Marathon transforms. Possible additional contributors to the occurrence of anomalous earthquakes include recent changes in plate motion, differential lithospheric cooling, and the development of a zone of weakness along the fault zone, but we do not find strong evidence to confirm the influence of these processes.

INTRODUCTION

Since Sykes's [1967] study of earthquakes on mid-ocean ridges confirmed the transform fault hypothesis [Wilson, 1965], the mechanisms of most earthquakes along oceanic transforms have been generally well-explained by a simple model. Such earthquakes are expected to have strike-slip mechanisms consistent with transform motion, to have vertical or nearly vertical fault planes, and to occur on the principal transform displacement zone (PTDZ). A corollary of this standard model, from the classical theory of faulting [Anderson, 1951], is that the direction of the most compressive principal stress σ_1 is horizontal and makes an angle of about 30° (on the basis of laboratory-derived coefficients of friction [Byerlee, 1978]) to the strike of the fault. Two current lines of research, however, suggest that this model bears closer scrutiny. First, studies of earthquake characteristics and fault mechanics along oceanic [Prothero and Reid, 1982; Tréhu and Solomon, 1983; Bergman and Solomon, 1988] and continental transforms [e.g., Segall and Pollard, 1980; King and Nabelek, 1985; Sibson, 1985, 1986; Nabelek et al., 1987; Barka and Kadinsky-Cade, 1988; Saucier et al., 1992] have shown that bends or offsets in the fault can strongly affect the state of stress and

pattern of earthquake faulting near such features. Second, there is increasing evidence that at least some oceanic and continental transforms act as weak zones relative to the adjacent lithosphere and that the stress state near the fault departs from classical theory [Zoback et al., 1987; Mount and Suppe, 1987; Wilcock et al., 1990]. In this paper, we present new information from a study of oceanic transform earthquakes with unusual mechanisms or locations confirming that a vertical strike-slip fault along the PTDZ is not always an adequate model for transform geometry and slip.

Recent studies of individual oceanic transforms with high-resolution bathymetric mapping, side-scan sonar imaging, and observations from submersibles have revealed complex fault geometries and structures within the transform domain [Fox and Gallo, 1984, 1986]. Extensional or compressional jogs (bends or offsets) in the PTDZ have been documented along several transforms [e.g., Macdonald et al., 1979, 1986; Lonsdale, 1986; Gallo et al., 1986; Fornari et al., 1989]. Microearthquake experiments conducted with ocean bottom seismometers have indicated patterns of seismicity and fault plane solutions consistent with the presence of extensional relay zones along the Rivera [Prothero and Reid, 1982] and Orozco [Tréhu and Solomon, 1983] transforms. Large earthquakes occurring near compressional fault jogs on the Kane and Vema transforms in the Atlantic have been shown to consist of primary strike-slip events and secondary events with reverse faulting mechanisms [Bergman and Solomon, 1988]. Engeln et al. [1986] also noted eight Atlantic transform earthquakes with apparently shallowly dipping fault planes or a dip-slip component of displacement, but independent body waveform inversions have shown that two of these events are normal-faulting earthquakes occurring on the nearby ridge segment and one is a strike-slip earthquake on a steeply dipping plane with a smaller reverse-faulting precursor [Huang et al., 1986; Bergman and Solomon, 1988].

¹Now at U.S. Geological Survey, National Earthquake Information Center, Golden, Colorado.

²Now at Department of Terrestrial Magnetism, Carnegie Institution of Washington, D.C.

Copyright 1993 by the American Geophysical Union.

Paper number 93JB00887.
0148-0227/93/93JB-00887\$05.00

Studies of continental strike-slip faults have illustrated the importance of fault geometry on the pattern of faulting. Jogs in strike-slip faults are known to produce uplift or subsidence along the fault, depending of whether the sense of the jog is compressional or extensional [Sylvester, 1988; Bilham and King, 1989; Anderson, 1990]. Earthquake rupture can be stopped by both compressional and extensional jogs [Segall and Pollard, 1980; King and Nabelek, 1985; Sibson, 1985, 1986]. Numerical models of strike-slip faults that are offset or contain bends show that such geometry can considerably alter the state of stress [Segall and Pollard, 1980; Saucier et al., 1992]. For instance, the thrust faulting component to the mechanism of the Loma Prieta earthquake has been attributed to the event's location at a local bend in the San Andreas fault in the Santa Cruz Mountains [McNally et al., 1989]. In the North China Basin [Nabelek et al., 1987] and along strike-slip faults in Turkey [Barka and Kadinsky-Cade, 1988] earthquake mechanisms and locations in conjunction with geologic information indicate normal faulting at extensional jogs and reverse faulting at compressional jogs.

The orientation of stresses in central California, as inferred from borehole breakout data, off-fault focal mechanisms, and the trends of active reverse faults and thrust-related anticlines along the fault system, indicate that σ_1 is nearly perpendicular to the San Andreas fault within only a few kilometers of the fault zone [Zoback et al., 1987; Mount and Suppe, 1987; Jones, 1988]. Such an orientation differs from that of the stress field farther (~100 km) from the fault. The lack of a heat flow anomaly across the San Andreas fault requires that shear stresses acting on the fault plane be low, less than about 20 MPa [Brune et al., 1969; Lachenbruch and Sass, 1980]. These results, and a small predicted component of convergence between the Pacific and North American plates, have led to the suggestion that plate motion along the San Andreas is decoupled by a weak fault zone into a low-stress, strike-slip component along the fault and a high-stress, compressional component off the fault [Zoback et al., 1987; Mount and Suppe, 1987].

The orthogonality of ridge-transform plate boundaries suggests that oceanic transforms are also comparatively weak. A perpendicular ridge-transform-ridge configuration minimizes the energy dissipated along the plate boundary if the transform is a zone of weakness, i.e., if stresses resisting plate separation along the ridge axis are larger than the shear stresses along the transform [Lachenbruch and Thompson, 1972; Froidevaux, 1973; Stein, 1978]. Curvature of the ridge axis neovolcanic zone toward the transform fault as the ridge-transform intersection is approached is also consistent with ridge axis stresses being several times larger than shear stresses on the transform [Phipps Morgan and Parmentier, 1984]. Fracture zone bathymetry and magnetic anomalies indicate that oceanic transforms are zones of weakness that adjust to changes in plate motion and can be deformed by compression or extension [Menard and Atwater, 1968]. In a microearthquake experiment along the active transform portion of the Kane Fracture Zone, Wilcock et al. [1990] observed that while the PTDZ was inactive during the experiment, seismic activity near the base of the southern transform valley wall was characterized by normal faulting, with the axis of least compressive stress σ_3 oriented perpendicular to the transform. Such a stress state is consistent with the hypothesis that the transform acts as a zone of weakness.

To investigate further the nature of shear stress and deformation in the vicinity of oceanic transform faults, we have conducted a

global search of large (body wave magnitude $m_b \geq 4.5$) earthquakes on and near oceanic transforms for those events with unusual source mechanisms and locations. From an initial examination of the Harvard catalogue of centroid moment tensor (CMT) solutions [Dziewonski et al., 1981], we identified transform earthquakes with mechanisms differing from the expected model of strike-slip motion on a vertical fault. We limit the present study to seven transforms on which we found anomalous earthquakes suitable for further study using an inversion of long-period body waveforms [Nabelek, 1984]. To provide better constraints on the pattern of seismicity and its relation to fault geometry, we relocated earthquakes along these transforms with a multiple-event relocation technique [Jordan and Sverdrup, 1981]. We consider the implications of these results for the standard fault model for transform slip, for the importance of geometrical irregularities in the fault trace, and for the state of stress near and along transforms.

A SEARCH FOR EVENTS WITH ANOMALOUS MECHANISMS

The search of the Harvard CMT catalogue for 1977-1989 for oceanic transform events with mechanisms differing significantly from the prediction of the standard model was conducted as follows. Earthquake epicenters from the catalogue of the International Seismological Centre (ISC) for 1964-1989 served to define the geometry of the ridge-transform system. Transforms are identified by the trend of ISC epicenters and strike-slip mechanisms with the expected sense of motion. For large-offset transforms, on which there is a significant amount of earthquake activity, this means of identification is adequate. Figure 1 shows a sample map of earthquake epicenters and CMT mechanisms along the active portion of the Eltanin Fracture Zone, made up of three transforms

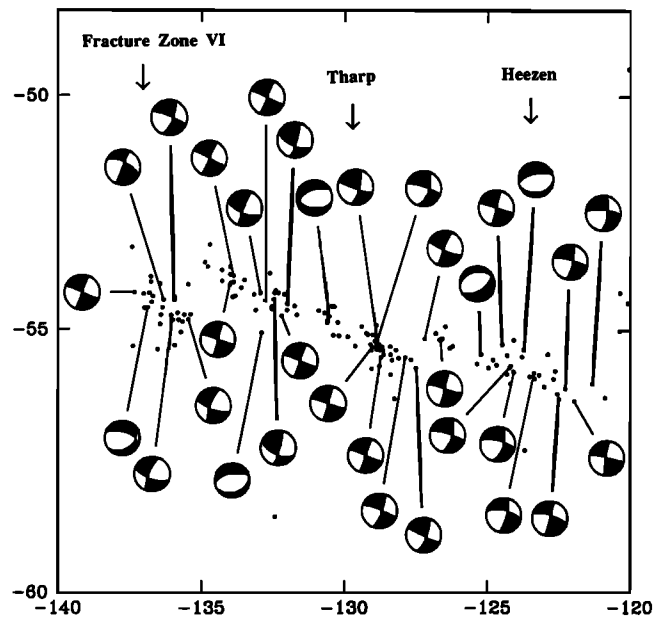


Fig. 1. Earthquake epicenters (International Seismological Centre (ISC)) and centroid moment tensor (CMT) mechanisms for earthquakes along the Eltanin fault system on the Pacific-Antarctic plate boundary. Epicenters are depicted by dots; mechanisms are equal-area projections of the lower focal hemisphere, with compressional quadrants shaded. The Eltanin system is made up of the Heezen and Tharp transforms and a transform identified as Fracture Zone VI by Molnar et al. [1975].

along the Pacific-Antarctic plate boundary; several anomalous normal-faulting mechanisms are evident in this region. We excluded from this study areas where the ridge approaches a trench or a continent (e.g., the Gulf of California and the Gulf of Aden). There is possible bias in the search procedure in that earthquakes that displayed normal-faulting mechanisms and occurred near the ridge-transform intersection with one or both nodal planes oriented parallel to the ridge axis were assumed to be related to the spreading process.

We identified 15 large-offset oceanic transform faults where earthquakes with anomalous mechanisms occurred during the 13-year study interval (we include the Udintsev transform in this list, where an anomalous strike-slip earthquake occurred in 1990). The mechanisms vary from reverse, to normal, to strike-slip with the wrong sense of slip for transform motion. Only 10 of these earthquakes (occurring on seven transforms) are well-enough recorded to permit body waveform inversion. Table 1 lists the source parameters derived for these earthquakes. The CMT source parameters of other anomalous transform earthquakes are listed in Table 2. Figure 2 shows the location of the seven transforms that we have investigated in detail.

WAVEFORM INVERSION

In CMT analysis [Dziewonski *et al.*, 1981; Dziewonski and Woodhouse, 1983], long-period digital waveforms are inverted for

the six independent components of the moment tensor, as well as centroid origin time and location. The inversion includes all seismic phases that arrive at a station prior to the arrival of Rayleigh or Love waves (for earthquakes having scalar moment M_0 greater than about 1×10^{25} dyn cm long-period mantle waves are included). Data are filtered to exclude periods less than 45 s and do not constrain shallow centroid depths. In addition, for shallow earthquakes the components of the moment tensor corresponding to a vertical dip-slip or horizontal thrust mechanism are the least well resolved.

We have refined the mechanisms and centroid depths of the anomalous transform earthquakes using an inversion of long-period teleseismic P and SH waveforms [Nabelek, 1984] from stations of the World-Wide Standardized Seismograph Network (WWSSN). Because long-period WWSSN instruments have peak responses at 15-s period, this inversion can usually constrain the centroid depth and the vertical dip-slip or horizontal strike-slip component of shallow earthquakes [Nabelek, 1984]. (However, CMT solutions are more sensitive to data at longer periods and better describe the seismic moment.) For 13 earthquakes, there is a good azimuthal distribution of stations with clear P and S arrivals on WWSSN analogue records. WWSSN records were digitized and corrected for differences in magnification and epicentral distance as described by Bergman *et al.* [1984]. Global Digital Seismic Network (GDSN) S wave data were included when necessary to improve SH coverage. In a few cases, additional P

TABLE 1. Epicentral Data and Source Parameters From Body Waveform Inversion

Date	Origin Time, ^a UT	Latitude, ^a N	Longitude, ^a E	m_b^a	M_S^a	M_0^b	Mechanism ^c	Depth, ^d km	STF, ^e s
<i>Carlsberg Ridge: Owen Transform</i>									
Sept. 29, 1983	1803:59.8	10.45	56.91	5.7	5.0	2.0×10^{24}	214/89/298	11	4
Sept. 7, 1986	1626:56.5	10.31	56.81	6.2	6.1	3.7×10^{25}	238/36/095	4	8
<i>Mid-Atlantic Ridge: St. Paul's Transform</i>									
Oct. 11, 1973	0207:51.8	0.52	-29.47	5.9		6.2×10^{25}	264/82/183	12	11
Oct. 14, 1982	1729:24.7	0.99	-29.07	5.1	5.2	9.0×10^{24}	86/66/172	11	5
Oct. 12, 1985	2220:42.8	0.87	-29.90	5.4	5.9	4.2×10^{25}	76/72/174	10	17
Sept. 20, 1986	0131:14.2	0.88	-29.25	5.4	4.8	1.8×10^{24}	227/53/050	14	3
Apr. 4, 1988	0425:36.7	0.97	-30.27	5.8	5.4	2.7×10^{24}	189/52/107	8	3
Dec. 23, 1988	2149:09.1	0.77	-29.41	5.7	5.5	6.0×10^{24}	228/56/072	9	4
<i>Mid-Atlantic Ridge: Marathon Transform</i>									
Sept. 22, 1985	1823:12.9	12.52	-44.31	5.6	5.5	4.2×10^{24}	140/54/051	4	4
<i>Pacific-Antarctic Ridge: Heezen Transform</i>									
Feb. 17, 1978	0140:03.1	-55.71	-125.24	5.7	5.2	2.4×10^{24}	241/16/309	11	3
<i>Pacific-Antarctic Ridge: Tharp Transform</i>									
May 27, 1989	0301:24.7	-55.24	-133.14	5.5	5.7	1.5×10^{25}	275/59/287	12	7
<i>East Pacific Rise: Menard Transform</i>									
May 15, 1987	1349:14.6	-49.91	-115.3	5.5	4.7	1.9×10^{24}	50/37/247	9	2
<i>East Pacific Rise: Rivera Transform</i>									
Sept. 21, 1977	1315:58.2	19.97	-109.26	5.5		4.9×10^{24}	353/35/291	4	6

^aEpicentral data, m_b , and M_S are from the International Seismological Centre.

^bSeismic moment in units of dyne centimeters.

^cStrike/dip/slip, in degrees, using the convention of Aki and Richards [1980].

^dDepth of centroid below the seafloor.

^eDuration of the source time function (STF).

wave coverage was gained by using broad-band seismograms constructed by combining long-period and short-period GDSN data in the frequency domain [Harvey and Choy, 1982]. For such a construction we used a procedure similar to that of Ekström [1989]; short-period data were resampled at 0.2 s and broad-band data were filtered with a three-pole band-pass Butterworth filter with corner frequencies at 0.015 and 1.0 Hz.

The source parameters in the inversion are centroid depth, double-couple mechanism, seismic moment, and the source time function (STF). The number of elements in the STF, taken as a series of overlapping triangles, is assigned prior to inversion and represents an additional parameter to be tested. In some cases the event is parameterized as two point sources or as a unilateral, horizontally propagating rupture along the strike of one of the nodal planes. For the latter situation a rupture velocity of 3.5 km/s is assumed. Values for the attenuation parameter t^* [Futterman, 1962] are taken to be 1.0 s for long-period P waves and 4.0 s for long-period S waves.

The assumed source velocity structure has an effect on the inversion results, in that takeoff angles of the rays and delay times

of depth phases depend on the source structure. For slow slipping transforms, we adopted the velocity structure used by Bergman and Solomon [1988], which was based on the refraction studies of Bowen and White [1986] and Loudon et al. [1986] of the Vema transform (Table 3). For fast slipping transforms, data on the velocity structure are limited: a study at the Orozco transform [Tréhu and Purdy, 1984] found anomalous velocity structure associated with relict ridge features and normal oceanic crust to the south of the transform. A model for normal oceanic crust (Table 3) was used for the source region along fast slipping transforms.

Body wave modeling has proven useful in determining the centroid depths of earthquakes in a number of tectonic settings, but the uncertainty in depths determined with this method is often difficult to establish. Discussions of the errors in determining centroid depths are given by Nabelek [1984], Huang et al. [1986], Stein and Wiens [1986], Goff et al. [1987], and Bergman and Solomon [1988]. Factors such as signal-to-noise (S/N) ratio, station distribution, mechanism, and depth of faulting can all influence the magnitude of uncertainties.

For all events, we conducted a series of inversions with the

TABLE 2. Epicentral Data and Centroid Moment Tensor Source Parameters of Additional Unusual Transform Earthquakes

Date	Origin Time, ^a UT	Latitude, ^a °N	Longitude, ^a °E	M_0 ^b	Mechanism ^c	Source
Oct. 8, 1980	2019:47.0	-4.87	-106.15	4.55×10^{24}	280/72/197	Dziewonski et al. [1988a]
<i>East Pacific Rise: Gofar Fracture Zone</i>						
Aug. 16, 1984	1530:59.8	-55.40	-123.75	1.57×10^{24}	257/63/268	Dziewonski et al. [1985]
<i>Pacific-Antarctic Ridge: Heezen Transform</i>						
Oct. 10, 1982	1744:45.2	-54.73	-130.54	6.18×10^{23}	246/54/250	Dziewonski et al. [1988c]
<i>Pacific-Antarctic Ridge: Tharp Transform</i>						
Sept. 17, 1982	1108:31.7	-54.55	-136.86	6.65×10^{23}	287/61/298	Dziewonski et al. [1983a]
<i>Pacific-Antarctic Ridge: Fracture Zone VI</i>						
Nov. 1, 1990	0156:44.6	-56.00	-143.19	8.04×10^{23}	264/90/180	Dziewonski et al. [1991]
<i>Pacific-Antarctic Ridge: Udintsev Transform</i>						
May 28, 1977	1510:13.6	-65.04	175.71	4.16×10^{24}	153/46/129	Dziewonski et al. [1987a]
<i>Pacific-Antarctic Ridge: Unnamed Transform</i>						
June 20, 1983	2241:57.3	-42.82	83.57	4.97×10^{23}	247/49/134	Dziewonski et al. [1983b]
<i>Southeast Indian Ridge: Unnamed Transform</i>						
May 5, 1988	2335:34.7	-49.82	115.38	4.03×10^{24}	112/69/130	Dziewonski et al. [1989b]
<i>Southeast Indian Ridge: Unnamed Transform</i>						
Aug. 17, 1977	1041:40.3	-40.95	42.70	8.00×10^{23}	145/58/070	Dziewonski et al. [1987a]
<i>Southwest Indian Ridge: Discovery II Transform</i>						
Sept 29, 1986	0710:37.7	10.58	57.05	7.47×10^{23}	242/72/167	Dziewonski et al. [1987b]
<i>Carlsberg Ridge: Owen Transform</i>						
Oct. 17, 1987	0812:21.4	43.30	-126.65	1.52×10^{24}	28/90/078	Dziewonski et al. [1989a]
Jan. 11, 1989	1223:33.1	44.60	-129.69	4.52×10^{23}	140/48/262	Dziewonski et al. [1990a]
<i>Juan de Fuca Ridge: Blanco Transform</i>						
Dec. 30, 1989	2016:02.2	1.00	-30.15	6.85×10^{23}	304/90/000	Dziewonski et al. [1990c]
<i>Mid-Atlantic Ridge: St. Paul's Transform</i>						

^aEpicentral data, m_b , and M_S are from the International Seismological Centre, except that data for the earthquake of November 1, 1990, are from the National Earthquake Information Center's Preliminary Determination of Epicenters.

^bSeismic moment in units of dyne centimeters.

^cStrike/dip/slip, in degrees, using the convention of Aki and Richards [1980].

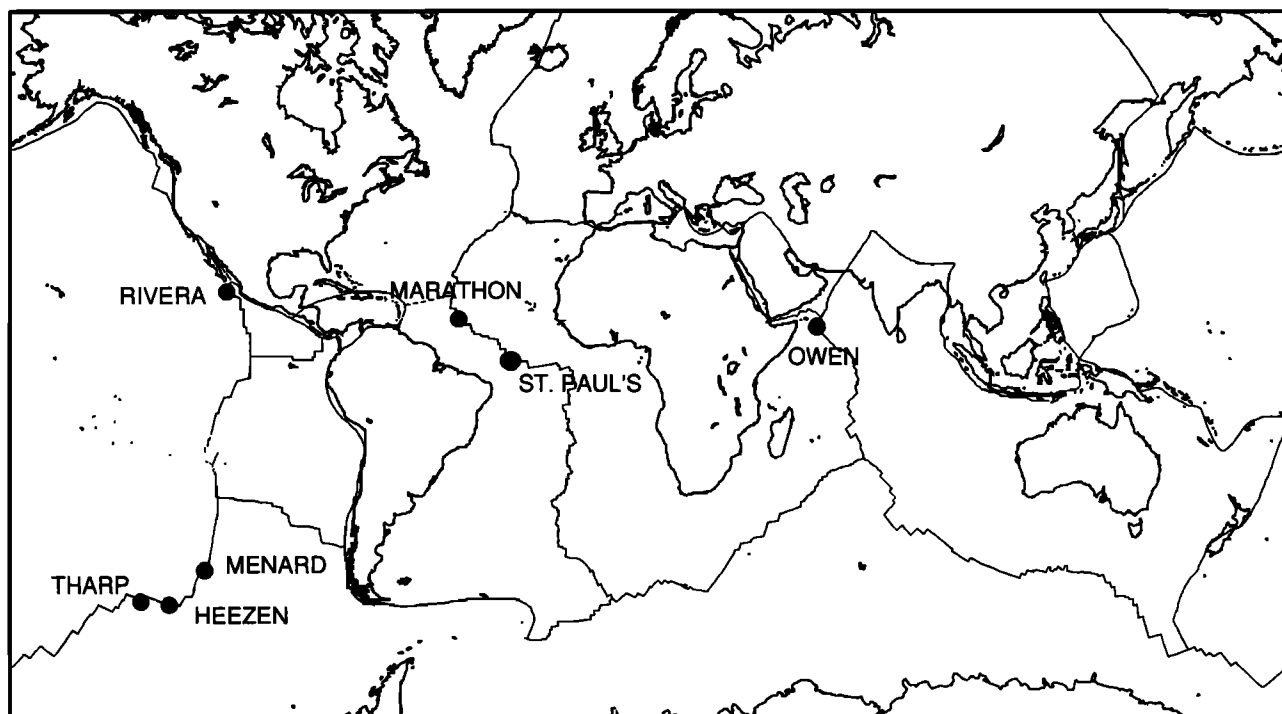


Fig. 2. Location of the seven transforms considered in this study. Locations of the earthquakes along these transforms with anomalous mechanisms and for which we have performed body waveform inversion are shown as solid circles. Also shown are plate boundaries and continents in Mercator projection.

depth fixed at values spanning a wide range; at each depth we solved for the remaining source parameters. The alignment between observed and synthetic seismograms and the length of the STF are both critical elements in this process. Seismograms are checked for proper alignment during each inversion, and STF lengths are chosen so that the final element tends toward zero amplitude. Our estimates of centroid depths are based on the interval over which the residual variance, given by the weighted mean squared difference between the observed and synthetic waveforms divided by the data variance (weighted mean squared observed waveforms), is minimized [Huang *et al.*, 1986]. While Huang *et al.* [1986] developed formal estimates of depth resolution using a statistical approach, Bergman and Solomon [1988] suggest that the range in centroid depth over which the residual variance varies by no more than a small percentage of the data variance also allows a simple yet conservative estimate of the uncertainty in centroid depth. The presence of distinguishable depth phases provides another important constraint on centroid depths. However, apparent depth phases can be generated either by surface reflections from a simple source or by a source at a shallower depth with a complex STF. Within a range of minimum residual variance, we prefer solutions for which the STF is single-peaked and matches depth phases.

The results of the waveform inversions are given in Table 1. The inversions for individual events are discussed in the appendix.

EARTHQUAKE RELOCATIONS

We applied a multiple-event relocation technique [Jordan and Sverdrup, 1981] to study the pattern of seismicity in the vicinity of unusual transform events. The advantage of a multiple-event relocation is its ability to reduce the effect of path-correlated noise on the relative locations of earthquakes within a small region. In

the hypocentroidal decomposition method of Jordan and Sverdrup [1981], an inversion for the relative locations between events (the cluster vectors) is performed first, and then the global position of the average location of events within a cluster (the hypocentroid) is determined. This technique has advantages over other methods for multiple-event location in that it does not require fixing a master event and it makes full use of all available data.

This method is well suited for studying the relative locations of oceanic events with teleseismic data [Jordan and Sverdrup, 1981; Bergman and Solomon, 1990; Wiens and Petroy, 1990]. As with the single earthquake location problem, the epicentroid can be biased by errors in the theoretical travel times and uneven station distribution. Bergman and Solomon [1990] found by comparison with epicenters from a local ocean bottom seismograph network

TABLE 3. Seismic Velocity Models Assumed for Source Regions

Layer	Thickness, km	V_P , km/s	V_S , km/s	ρ , g/cm ³
Fast Slipping Transforms				
1	variable	1.5	0.0	1.0
2	6.0	6.4	3.7	2.8
3	half-space	8.1	4.6	3.4
Slow Slipping Transforms				
1	variable	1.5	0.0	1.0
2	2.2	4.3	2.5	2.5
3	2.6	5.9	3.4	2.6
4	half-space	8.1	4.6	3.4

V_P and V_S are the P wave and S wave velocity, respectively; ρ is the density.

that the teleseismic epicentroid of a cluster of events on the northern Mid-Atlantic Ridge may be biased systematically to the north by as much as 15 km because of the concentration of stations in North America and Europe. The relative pattern of multiple-event locations tends to be less affected by such systematic error, although station distribution for individual events still affects the axis orientation and aspect ratio of confidence ellipses, and errors may be significant for earthquakes with few arrivals in a single quadrant.

The ISC catalogue for January 1964 to March 1989 was searched for earthquakes near each of the transforms of interest. We excluded events that could not be reliably located, for example events with fewer than seven arrival times or events with data in less than three azimuth quadrants. Details of the data selection and inversion procedures, including the travel time calculation, ellipticity correction, and weighting of the data, were generally as described by *Bergman and Solomon* [1990]. The stations in the inversion were constrained to be within epicentral distances of 20° to 98° . Focal depths were fixed at 10 km below sea level. The relocation procedure drops data with residuals greater than 10 s in the first iteration and then uses 3 s as a maximum residual. The relocation procedure is repeated so that data with large relative errors can be flagged and omitted in the next inversion for relative location, although all such data are included in the final hypocentroidal inversion.

Examples of the relative positions of relocated earthquakes, including 95% confidence ellipses, at the Heezen and St. Paul's transforms are shown in Figure 3. The absolute positions of all relocated earthquakes are plotted in Figures 4-10.

TRANSFORM FAULTS WITH UNUSUAL EARTHQUAKE MECHANISMS AND LOCATIONS

The anomalous transform mechanisms analyzed in this study occurred on seven oceanic transform faults along both slow and fast spreading ridges (Figure 2). In this section we present a synthesis of earthquake mechanisms and relocated epicenters on these oceanic transforms and of the relation of the earthquake characteristics to the geometry and structure of the transform fault zone.

Owen Transform

The Owen transform offsets the Carlsberg Ridge and the Sheba Ridge by 300 km. The present plate configuration was established at 10 Ma, when magnetic anomalies indicate that spreading in the Gulf of Aden commenced [*Laughton et al.*, 1970; *Cochran*, 1981]. The boundary of a magnetic quiet zone, marking the limit of recent spreading on the Sheba Ridge, is presently located about 150 km from the ridge [*Cochran*, 1981], only halfway along the transform. *Stein and Cochran* [1985] argue on the basis of basement depths and heat flow measurements that the Error Ridge complex and the Sharbithat Ridge complex, which border the magnetic quiet zone, were formed by rifting of old oceanic lithosphere during the early stages of opening of the Gulf of Aden. Changes in the trend of the inactive limbs of the fracture zone are also observed near its intersection with Error Ridge [*Matthews*, 1966; *Cochran*, 1981] and Sharbithat Ridge [*Whitmarsh*, 1979].

Three earthquakes with unusual mechanisms have occurred on the southwestern portion of the transform fault zone in the vicinity of Error Ridge (Figure 4): the thrust-faulting event of July 7, 1986, the vertical dip-slip (or low-angle strike-slip) event of July

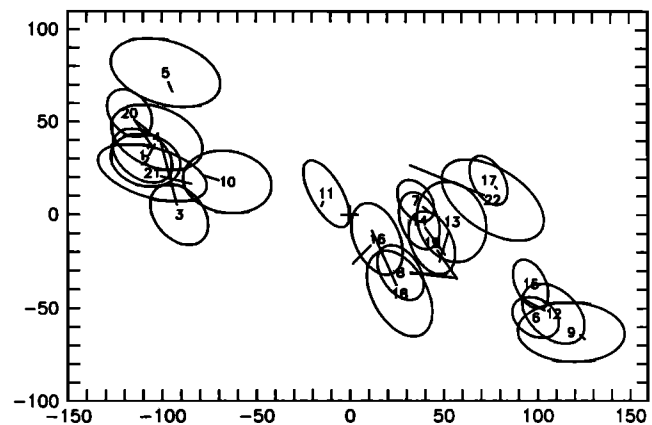


Fig. 3a. Relative locations of earthquakes (1964 to March 1989) on a central portion of the Heezen transform. For each earthquake the relative location is indicated by the event number, the 95% confidence ellipse for the cluster vector is shown, and the change in relative position from the starting (ISC) location is indicated by a line. The position of the average location of events within a cluster (the hypocentroid) is indicated by a cross. The distance scales are in kilometers north and east of the hypocentroid. Events are numbered in chronological order.

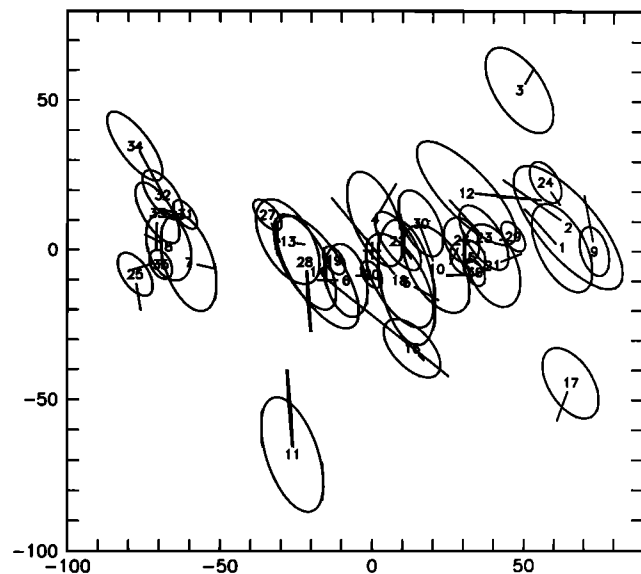


Fig. 3b. Relative locations of earthquakes on the western portion of the St. Paul's transform (ISC locations west of 29°W).

29, 1983, and the September 29, 1986, event having a strike-slip mechanism with an unusual fault orientation. In relocating earthquakes using the multiple-event technique, the assumption that *P* waves have traveled similar paths begins to break down at interevent distances larger than perhaps 200-300 km. We therefore divided the large area around the southwestern ridge-transform intersection into three regions, and we relocated subsets of earthquakes on the ridge, at the ridge-transform intersection, and on the central portion of the transform. The September 29, 1986, earthquake is one of a series of aftershocks northwest of the large ($M_0 = 2 \times 10^{25}$ dyn cm) strike-slip main event of September 17, 1986. Three earthquakes occurred after the July 7, 1986, earthquake, two on the transform, one on the ridge. Body waveform inversions for the July 29, 1983, and July 7, 1986, earthquakes are given in the appendix (Figures A1 and A2).

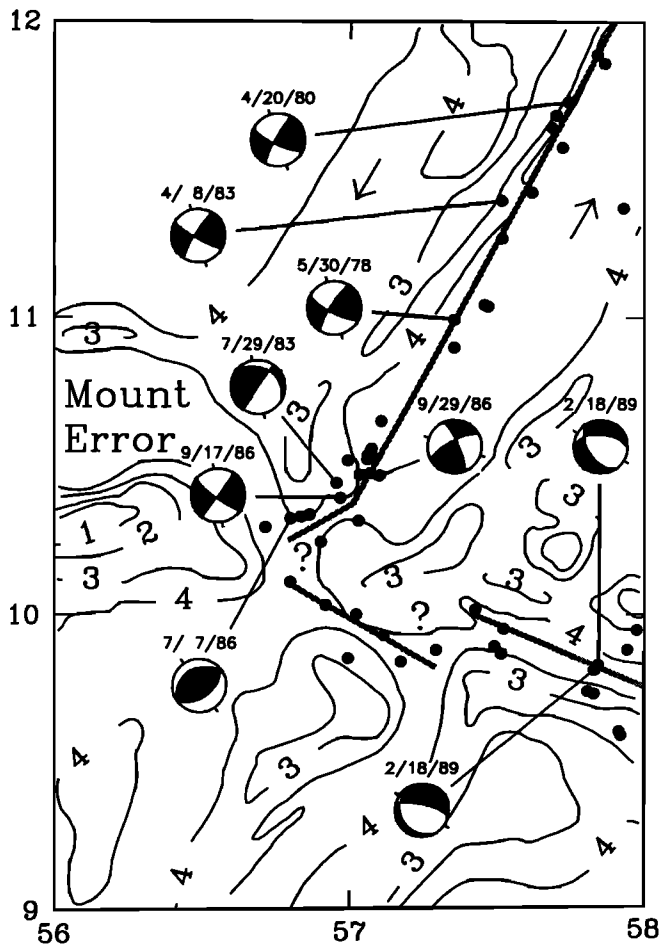


Fig. 4. Earthquake locations and mechanisms along the southwestern portion of the Owen transform. Bathymetry is adapted from Cochran [1988]; 1-km contour interval. Mount Error is at about 10.3°N , 56.2°E and reaches depths of < 1 km. The southeastern portion of Error Ridge includes both Mount Error and the elongate high at about 11°N , 56.2°E . Suggested plate boundary geometry is shown as a stippled line; question marks show portions of the boundary where the geometry is poorly constrained. The northeastern transform boundary is taken as a small circle about the African-Indian Euler vector, and arrows denote relative plate motion directions [DeMets *et al.*, 1990]. Epicenters (solid circles) are of relocated events from January 1964 to March 1989. The mechanisms of the earthquakes of July 29, 1983, and July 7, 1986, are from this study. All other mechanisms are from the Harvard CMT catalogue. Tic marks denote the azimuth of the maximum compressive horizontal stress, under the assumption that the P axis and T axis correspond to the axes of maximum and minimum principal stress, respectively. This assumption may not always be valid [McKenzie, 1969].

In the vicinity of the ridge-transform intersection, the earthquake epicenters and the bathymetry indicate an apparent compressional jog (Figure 4), although the transform in this area may be made up of several faults accommodating slip. To the northeast of the jog, the slip vectors of the strike-slip mechanisms and the epicenters follow a linear trend defining the transform fault zone. The July 29, 1983, and September 17, 1986, earthquakes, located near the northeastern end of the jog, both have one nodal plane on which horizontal slip would be in the expected direction of transform motion. The mechanism of the September 29, 1986, aftershock, however, is incompatible with expected transform motion. The orientations of both nodal planes of the July 7, 1986, reverse-faulting earthquake are rotated clockwise from the transform-

parallel direction, a sense that is consistent with slip occurring at a compressional jog. The orientation of the maximum horizontal compressive stress indicated by the anomalous mechanism of the earthquake of July 29, 1983, is similar to that for most strike-slip events along the transform. The orientation of σ_1 for the September 29, 1986, earthquake indicates transform-perpendicular compression.

St. Paul's Transform

The three large equatorial transforms, the St. Paul's, the Romanche, and the Chain, offset the Mid-Atlantic Ridge by about 630, 940, and 300 km, respectively. In the central and eastern portion of the St. Paul's transform there are at least three volcanically active extensional relay zones [Schilling *et al.*, 1987]. A notable feature of this transform is the presence of St. Peter's and St. Paul's Rocks (hereafter referred to as just St. Paul's Rocks), a small group of nonvolcanic islets. While previous studies place the islets along a transverse ridge on the northern boundary of the transform, a revised bathymetric map indicates that the transform divides this feature (Figure 5). Studies have shown that St. Paul's Rocks consist mostly of mylonitized peridotite and hornblende and are likely an upper mantle-derived intrusion [e.g., Melson *et al.*, 1972]. Recent volcanism is postulated to have occurred north of St. Paul's Rocks, where an alkali basalt associated with Quaternary sediments and carrying mylonitized ultramafic xenoliths was dredged [Sinton, 1979].

Several earthquakes with unusual mechanisms and locations are found in the area around St. Paul's Rocks (Figure 5). Because the study area is large, we have relocated events in three smaller subsets, with one group containing the area of the ridge north of the transform intersection and two groups covering the western part of the transform. As can be seen directly in the elongation of the confidence ellipses (Figure 3b), the distribution of stations for these events gives poorest epicentral resolution in the northwest to southeast direction. Events with anomalous locations (on October 11, 1973, November 14, 1982, and October 12, 1985) or CMT mechanisms (on September 20, 1986, April 20, 1988, and December 23, 1988) were selected for further study using waveform inversion. Data are not yet available for the earthquake of December 30, 1989, but this event had a small moment (7×10^{23} dyn cm) and likely cannot be analyzed by body waveform inversion with WWSSN data.

The orientation of the greatest horizontal compressive stress indicated by the mechanisms of the two reverse-faulting earthquakes of September 20, 1986, and December 23, 1988, are similar, although rotated to more nearly perpendicular to the transform than the directions given by the strike-slip events. We postulate that these earthquakes may be associated with a small compressional jog in the vicinity of St. Paul's Rocks and that the presence of anomalous structure has an influence on fault motion. Further information is needed on the fault geometry and transform structure near St. Paul's Rocks before this conjecture can be evaluated. The April 20, 1988, reverse-faulting earthquake shows a fault plane striking parallel to the ridge, and the direction of maximum horizontal compressive stress is transform-parallel (σ_2 is perpendicular to the transform); this event was followed by a series of aftershocks (events 32, 33, 34, and 35 in Figure 3b). The mechanism of the unusual strike-slip event of December 30, 1989, is consistent with a maximum horizontal compressional stress that is transform parallel in this region (and σ_3 perpendicular to the transform).

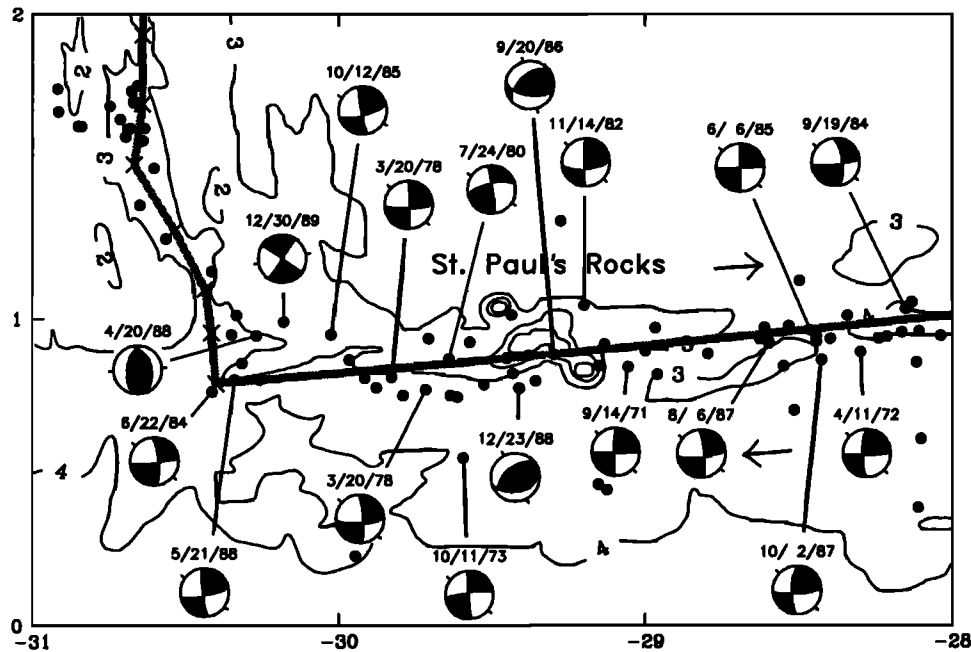


Fig. 5. Earthquake locations and mechanisms along the western portion of the St. Paul's transform. Bathymetric contours are from the General Bathymetric Chart of the Oceans (GEBCO) Digital Atlas, as supplied by the British Oceanographic Data Centre, Bidston, England, March 1992; 1-km contour interval, Mercator projection. The location of the December 30, 1989, event is from the ISC. Mechanisms of earthquakes on October 11, 1973; November 14, 1982; October 12, 1985; September 20, 1986; April 20, 1988; and December 23, 1988, are from this study. Mechanisms of the events on September 14, 1971, and April 11, 1972, are from *Engeln et al.* [1986]. Mechanisms of other events are taken from the Harvard CMT catalogue. Crosses show the location of the Mid-Atlantic Ridge and its intersection with the St. Paul's transform, as given by J.-G. Schilling (Lamont-Doherty Earth Observatory, unpublished cruise report, 1987). The transform boundary is taken as a small circle about the South American-African Euler vector [DeMets et al., 1990]. See Figure 4 for further details.

Seismic activity outside of the transform fault zone (Figure 5) between longitudes 29° and 30° W could be the result of the anomalous stresses in the vicinity of St. Paul's Rocks. The anomalous locations of the larger events, however, are more likely the result of travel time errors. For instance, the off-transform location of the October 11, 1973, earthquake (event 16 in Figure 3b) is strongly influenced by data from only two stations in the southern hemisphere; the event has a complicated source time function, which introduces large picking errors. The October 12, 1985, earthquake (event 27 in Figure 3b) has a long source time function; picking errors could again be large. The November 14, 1982, earthquake (event 24 in Figure 3b), with a simple STF, provides stronger evidence for deformation occurring outside the transform fault zone, slightly to the north of St. Paul's Rocks.

Marathon Transform

Between the Fifteen Twenty Fracture Zone and the Vema Fracture Zone, the Mid-Atlantic Ridge is offset by two smaller transforms, the Mercurius, which offsets the ridge by 45 km at $12^{\circ}10'N$, and the Marathon, which offsets the ridge by 80 km at $12^{\circ}40'N$ [Collette et al., 1979, 1980, 1984]. An anomalous reverse-faulting earthquake occurred on September 22, 1985, near the Marathon transform (Figure 6).

The ridge segments to the immediate north and south of the transform do not display recent seismic activity. Activity on the transform has been limited to the ridge-transform intersections, an area along the central portion of the transform, and a sequence of events to the southeast of the transform valley (Figure 6). The anomalous thrust earthquake of September 22, 1985, was the first

in a series of five events that occurred over a 4-day period on the southern transverse ridge. The period of the water reverberations in the P waveforms is consistent with a shallow water depth of 2-3 km.

Heezen and Tharp Transforms

The Heezen and Tharp transforms are two large-offset transforms on the fast spreading Pacific-Antarctic plate boundary, which is called the East Pacific Rise to the north and the Pacific-Antarctic Ridge to the south of these fracture zones. The Heezen and Tharp transforms are closely spaced (100 km), offset the ridge by 350 and 650 km, respectively, and collectively constitute most of the transform portions of the Eltanin Fracture Zone (Figure 1). The seismic history of the Eltanin system has been investigated by Stewart and Okal [1983], who suggested that seismic slip from 1920 to 1981 was about one tenth that predicted by plate motion models. They attributed the deficit to a lack of larger earthquakes, since there have been few earthquakes with $M_S > 6$ and none with $M_S > 7$.

Earthquakes with extensional mechanisms occur along both the Heezen and the Tharp transforms. Figure 7a shows relocated events along a central portion of the Heezen transform. A normal-faulting earthquake occurred on the transform on February 17, 1978 (event 11 in Figure 3a), and another occurred in a trough north of the transform on August 16, 1984 (event 17 in Figure 3a). Figure 8 shows relocated events along a central portion of the Tharp transform. A normal-faulting earthquake occurred on the transform on October 10, 1982. The May 27, 1989, normal-faulting earthquake is considered an intraplate event.

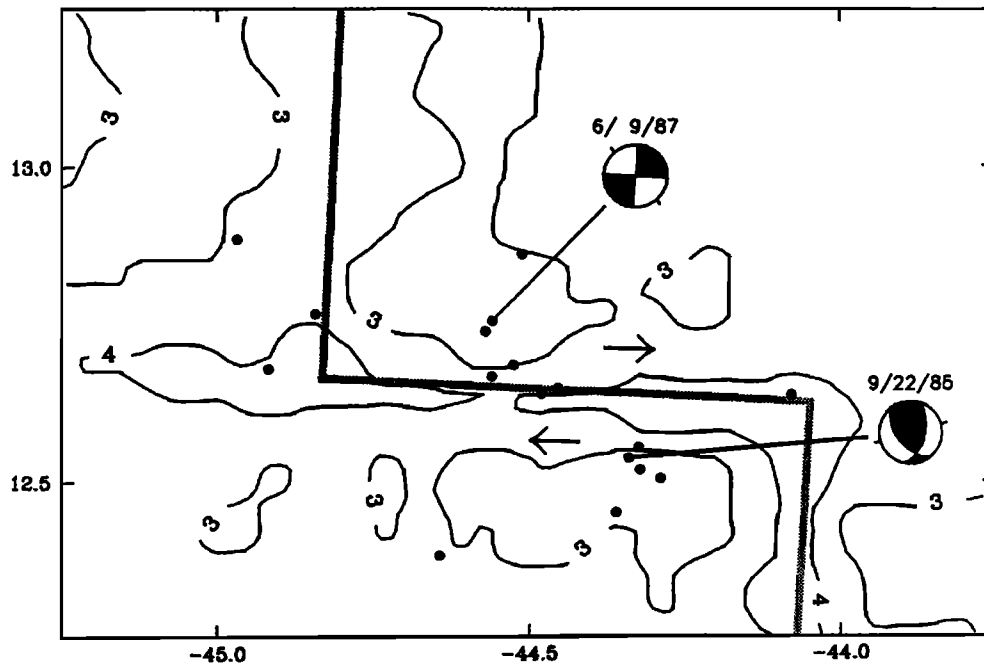


Fig. 6. Earthquake locations and mechanisms along the Marathon transform. Bathymetry is from Collette *et al.* [1984]; 1-km contour interval, Mercator projection. The mechanism of the September 22, 1985, earthquake is from this study. The June 9, 1987, mechanism is from the Harvard CMT catalogue. The transform boundary is taken as a small circle about the South American-African Euler vector [DeMets *et al.*, 1990]. See Figure 4 for further details.

The earthquakes of February 17, 1978, and May 27, 1989, were suitable for body waveform inversion (Figures A11 and A12). The August 16, 1984, earthquake on the Heezen transform and the October 10, 1982, earthquake on the Tharp display dilatational first motions on many short-period seismograms, consistent with the normal-faulting mechanisms indicated by CMT analysis.

A multibeam survey of a portion of the Heezen transform [Lonsdale, 1986] helps to identify the tectonic framework of the extensional events. Between 125°W and 126°W, there are three extensional offsets of the fault trace, with two of the offsets forming deep pull-apart basins [Lonsdale, 1986] (Figure 7b). The February 17, 1978, earthquake was located near the easternmost offset. The August 16, 1984, event occurred off the Heezen transform; a recent multibeam and side-scan sonar imaging survey of this area shows a transform-parallel trough that extends from the ridge (P. Lonsdale, personal communication, 1991).

The area of the Tharp transform near the epicenter of the October 10, 1982, normal-faulting earthquake has not been mapped with multibeam bathymetry. Because the pattern of earthquake seismicity is similar to that along the Heezen, however, we suggest that an extensional offset may be present along the Tharp transform in the vicinity of the epicenter.

Menard Transform

The Menard transform, north of the Eltanin system, is a large-offset transform on the fast spreading Pacific-Antarctic plate boundary. Bathymetric and geophysical data for this transform are given by Molnar *et al.* [1975]. A normal-faulting earthquake occurred along this transform on May 15, 1987 (Figure 9).

An apparent gap in seismicity about 50 km long occurs to the west of the anomalous event. Waveform inversion for the May 15, 1987, earthquake is given in Figure A13. The direction of

maximum horizontal compressive stress of the normal-faulting earthquake is similar to that of the strike-slip earthquakes.

Multibeam data from a recent survey indicate that a small extensional offset may be present at 116°W, where two parallel troughs, offset of by 1-2 km, overlap (P. Lonsdale, personal communication, 1991). The bathymetry within the Menard transform does not indicate the presence of a large extensional offset similar to that along the Heezen transform.

Rivera Transform

The current plate configuration at the Rivera transform was established around 3.5 Ma, when spreading ceased on the Mathematician Ridge and transferred to the Pacific-Cocos Rise [Klitgord and Mammerickx, 1982]. An abrupt change in orientation and tectonic character occurs midway along the transform near longitude 107.5°W. West of this area, seismicity is more diffuse, bathymetry exhibits greater relief, and the fracture zone consists of several subparallel valleys, although it is not known how slip is being accommodated among them [Ness and Lyle, 1991]. Teleseismically recorded earthquakes are generally smaller and more frequent in the western area, and there is a greater tendency for swarms to occur [Prothero and Reid, 1982]. DeMets and Stein [1990] find that the azimuths of the transform strike and earthquake slip vectors west of 108.3°W are systematically rotated by several degrees clockwise relative to the azimuths predicted by the Pacific-Rivera Euler vector. An extensional offset of the transform has been identified at 108°W on the basis of bathymetry and an en echelon pattern of microearthquakes [Prothero and Reid, 1982]. Prothero and Reid [1982] found a second en echelon offset of microearthquakes west of 109°W, possibly indicating another extensional relay.

Figure 10 shows relocated earthquakes ($m_b \geq 4.5$) and mechanisms along a portion of the western Rivera transform. The

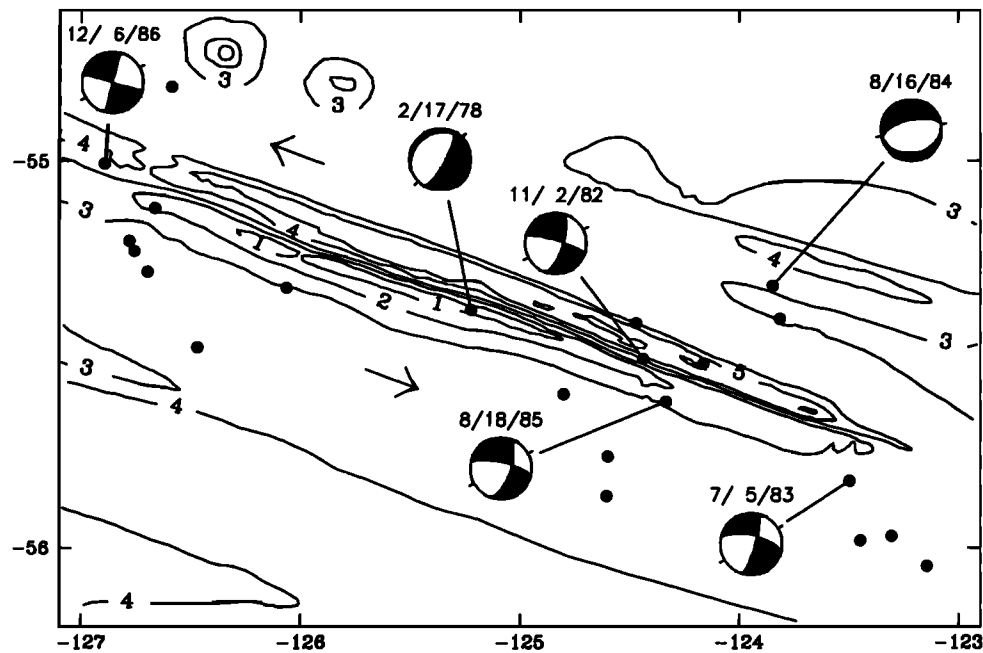


Fig. 7a. Earthquake locations and mechanisms along the central portion of the Heezen transform. Bathymetry is adapted from *Lonsdale* [1986]; 1-km contour interval. The mechanism of the earthquake of February 17, 1978, is from this study. All other mechanisms are from the Harvard CMT catalogue. See Figure 4 for further details.

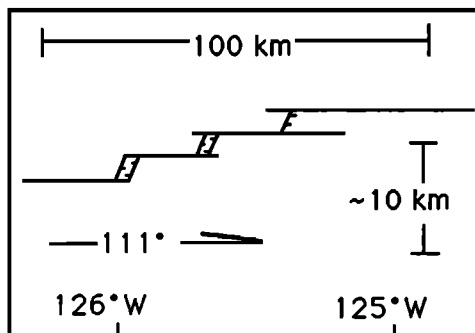


Fig. 7b. Geologic sketch map of the Heezen transform, adapted from *Lonsdale* [1986], oblique projection.

location uncertainty in the northeast-southwest direction is large because of a lack of arrivals to the southwest (epicentral confidence ellipses derived from multiple-event relocation are elongated in this direction). While most earthquake epicenters and mechanisms are consistent with the expected transform motion, to the west of 109°W some earthquake epicenters appear to lie north of the transform. This pattern occurs near the area where *Prothero and Reid* [1982] report an en echelon pattern of microearthquake epicenters.

Several earthquakes with anomalous mechanisms are located west of 109°W. The normal-faulting earthquake of September 21, 1977, occurred in the seismically active inner corner of the rise-transform intersection. In addition, three earthquakes with predominantly strike-slip mechanisms but with the strike directions of the probable fault planes rotated clockwise from the expected transform direction occurred on May 8, 1983. These earthquakes are a part of a sequence of about 15 events that span a 3-day period. The May 9, 1983, earthquake having a strike-slip mechanism with an anomalous fault dip is the largest event in this

sequence ($M_0 = 4.2 \times 10^{25}$ dyn cm). The earthquake of February 17, 1984, is located to the east of a short offset of the rise axis, a region where deformation may be more complex than simple strike-slip motion [*Lonsdale*, 1991]. The mechanism of this earthquake also shows a strike direction of the probable fault plane that is rotated clockwise from the expected direction of transform slip. Current bathymetric information does not permit a clear association of the unusual pattern of epicenters and mechanisms with morphologic features and physical processes.

CENTROID DEPTHS

Centroid depths of strike-slip earthquakes along the St. Paul's transform and the two reverse-faulting earthquakes near St. Paul's Rocks may be compared with results for other large earthquakes [*Engeln et al.*, 1986; *Bergman and Solomon*, 1988] and for microearthquakes [*Francis et al.*, 1978; *Wilcock et al.*, 1990] on slow slipping transforms. In contrast, centroid depths are not well resolved on the Heezen and Menard transforms because of the poor *P* wave S/N and the sparse sampling of waveforms. The age offset of the Owen transform is not fully developed, because oceanic crust generated by spreading on the Sheba ridge to the north extends only halfway along the transform, so the depth of seismic faulting cannot be simply related to thermal models.

From body waveform modeling, *Engeln et al.* [1986] reported centroid depths along Atlantic transforms from 2 to 7 km below the seafloor and suggested that earthquake faulting is limited by the 600°C isotherm. *Bergman and Solomon* [1988] disputed this result and on the basis of a more thorough waveform inversion procedure found that centroid depths on such transforms are generally 7-10 km, consistent with a nominal limiting isotherm of $900^\circ \pm 100^\circ\text{C}$. The centroid depths of 10-14 km that we determine for earthquakes along the St. Paul's transform are in agreement with the conclusions of *Bergman and Solomon* [1988]. To estimate the value of the isotherm limiting earthquake faulting, we follow the

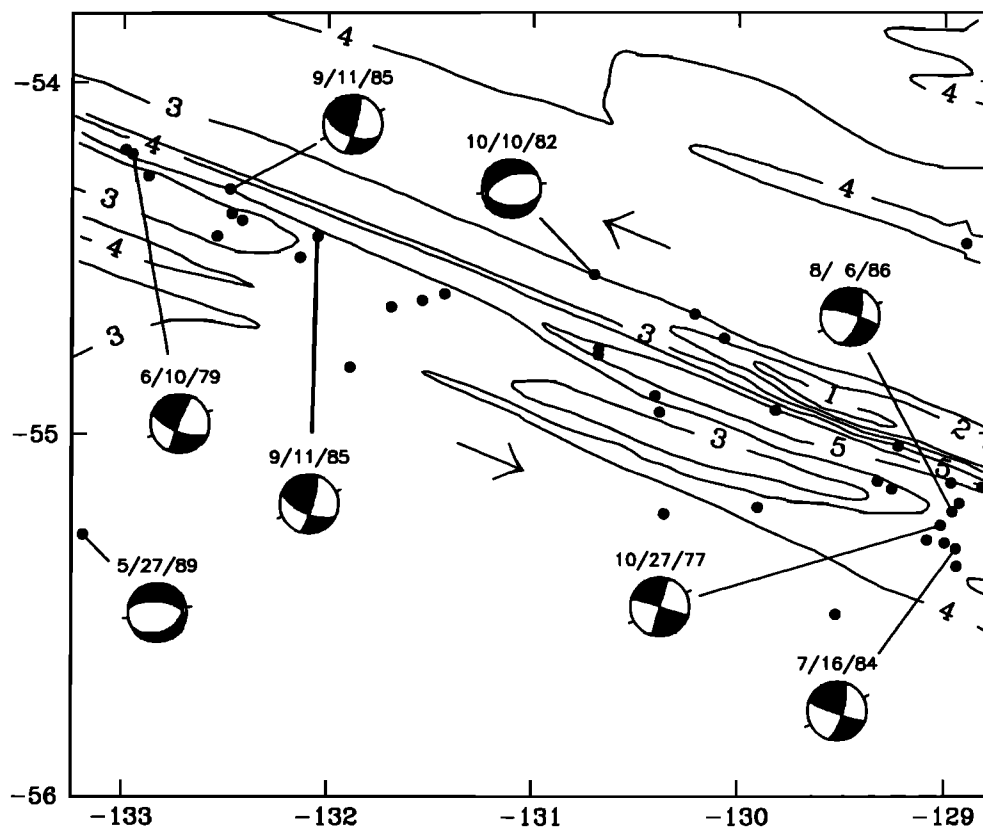


Fig. 8. Earthquake locations and mechanisms along a portion of the Tharp transform. Bathymetry is adapted from *Lonsdale* [1986]; 1-km contour interval. The mechanism of the May 27, 1989, earthquake is from this study. Other earthquake mechanisms are from the Harvard CMT catalogue. The epicenter of the May 27, 1989, earthquake is taken from the ISC catalogue. See Figure 4 for further details.

method of *Bergman and Solomon* [1988]: we average the isotherms in adjoining lithospheric plates, in which temperatures are calculated from a standard plate-cooling model [*Parsons and Sclater*, 1977], and we calculate the depth extent of faulting using the method of *Ebel et al.* [1978], which relates the radius of a circular fault to the duration of the source time function (further details are described by *Bergman and Solomon* [1988]). The depth extent of faulting is assumed to be twice the centroid depth for the two strike-slip earthquakes of October 11, 1973, and October 12, 1985, which have a calculated fault radius greater than the centroid depth.

The presence of volcanically active relay zones within the transform and the lack of magnetic anomaly information on age offset complicate specification of a thermal model. For a constant half-spreading rate of 16 mm/yr [*DeMets et al.*, 1990] and a fault offset of 630 km, the depth of faulting is limited by a temperature of $750^{\circ} \pm 100^{\circ}\text{C}$ (Figure 11a). If the fault offset is shortened to 300 km by postulating that volcanically active relay zones have thermal structures similar to fully developed ridge segments, the limiting isotherm may be as high as 1000°C (Figure 11b). However, since our thermal model neglects three-dimensional convective and conductive heat transfer across the transform, the thermal structure resulting from a short ridge segment within the long St. Paul's transform fault will differ from the two-dimensional approximation [e.g., *Phipps Morgan and Forsyth*, 1988]. When three-dimensional effects are considered, it is likely that the thermal effect of a short ridge will not be as extreme as predicted in Figure 11b.

The depths of microearthquakes are typically somewhat shallower than the inferred maximum depths of faulting of large earthquakes. From a microearthquake experiment at the eastern intersection of the St. Paul's transform and the Mid-Atlantic Ridge, *Francis et al.* [1978] found that earthquakes occurred in two depth intervals: shallow shocks at 0-1 km depth occurred mostly as small swarms on the ridge axis, while events clustered near 7 km depth occurred on the active transform. *Wilcock et al.* [1990] reported microearthquake focal depths along the Kane transform of 3-6 km near the ridge-transform intersection and 5-9 km in the transform fault zone distant from the intersection.

DISCUSSION

The mechanisms of transform earthquakes provide important information about mechanical processes occurring along the transform. In this section we evaluate the possible processes contributing to the occurrence of such events by comparing the characteristics of anomalous earthquakes to be expected from each process against our observations.

Importance of Fault Geometry and Structure

Bends or offsets in strike-slip faults are capable of generating anomalous stresses in the adjoining blocks, producing uplift or subsidence, and influencing the pattern of faulting [e.g., *Segall and Pollard*, 1980; *King and Nabelek*, 1985; *Sibson*, 1985, 1986; *Nabelek et al.*, 1987; *Barka and Kadinsky-Cade*, 1988; *Bilham and King*, 1989; *McNally et al.*, 1989; *Anderson*, 1990; *Saucier et al.*,

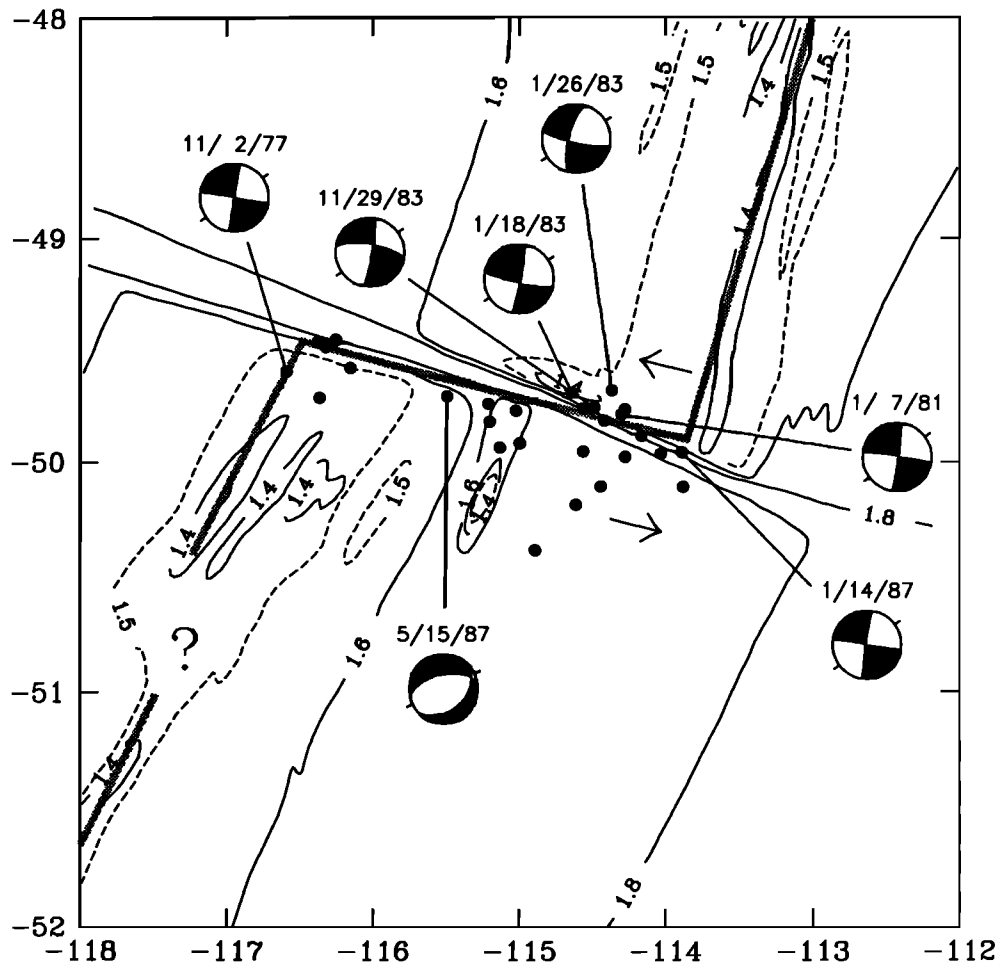


Fig. 9. Earthquake locations and mechanisms along the Menard transform. Bathymetry is adapted from *Mammerickx et al.* [1975]; contours are in thousands of fathoms, with a 100-fathom contour interval and the 1500-fathom contour dashed. The mechanism of the May 15, 1987, earthquake is from this study. Other earthquake mechanisms are from the Harvard CMT catalogue. The transform boundary is taken as a small circle about the Pacific-Antarctic Euler vector [*DeMets et al.*, 1990]. See Figure 4 for further details.

1992]. Previous studies [*Prothero and Reid*, 1982; *Tréhu and Solomon*, 1983; *Bergman and Solomon*, 1988] have shown that anomalous patterns of seismicity can also occur at bends or offsets in oceanic transforms. The observations of this study provide additional evidence that the presence of complex fault geometry and structure can influence the pattern of earthquake locations and mechanisms along oceanic transforms. Such irregularities in fault geometry can be expected to arise from a variety of processes influencing the temporal evolution of the PTDZ (e.g., changes in plate motion, diapiric rise of altered blocks of lower crustal or upper mantle material, volcanic construction, fault-normal compression or extension, variability in crustal accretion at adjoining ridge segments, or small deviations of transform strike from the ideal small circle).

At the western ridge-transform intersection of the Owen transform, as noted above, bathymetry, earthquake epicenters, and the presence of earthquakes with anomalous mechanisms indicate the existence of a compressional fault jog (Figure 4). The interaction of the active transform with Error Ridge, anomalous structure inherited from the opening of the Gulf of Aden, may account for the complex fault geometry.

At the St. Paul's transform, the reverse-faulting earthquakes occurring near St. Paul's Rocks (Figure 5) may be associated with

a compressive fault jog, similar to the case at the Owen transform. Elemental and isotopic chemistry, mineralogy, and geothermometry of islet samples suggest that St. Paul's Rocks may be a relict of subcontinental mantle, left behind in the opening of the Atlantic and subsequently emplaced as surface blocks [*Bonatti*, 1990]. While complexities in fault geometry may be responsible for the present deformation near St. Paul's Rocks, it is less likely that fault geometry was the principal cause for the original emplacement of this feature. Rapid ascent from depths greater than about 30 km and emplacement in the solid state are suggested by the presence of mantle-equilibrated primary assemblages in the form of augen within a variably recrystallized mylonite matrix [*Melson et al.*, 1972]. Uplifted blocks have been found on the walls of many transforms; petrologic investigations suggest that these blocks are made up of gabbro or peridotite that originated in the lower crust or upper mantle [e.g., *Bonatti*, 1978; *Bonatti and Hamlyn*, 1978].

Along the Pacific-Antarctic plate boundary, the normal-faulting earthquakes occurring on the Heezen, Tharp, and Menard transforms appear to be associated with extensional jogs in the trace of the PTDZ. At the Heezen transform, a normal-faulting earthquake occurred on the border of an extensional offset (Figure 7a), possibly reflecting a normal fault at the edge of a pull-apart basin. Normal-faulting earthquakes on the Tharp (Figure 8) and

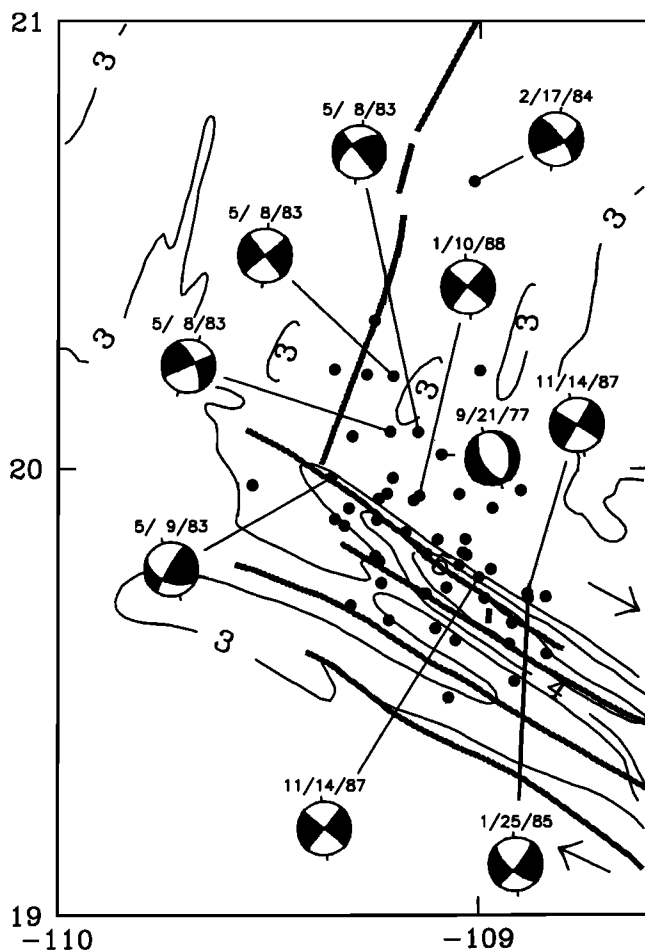


Fig. 10. Earthquake locations and mechanisms along the western Rivera transform. Bathymetry is adapted from *Dauphin and Ness* [1991]; 1-km contour interval. Plate boundary is taken from *Ness and Lyle* [1991], who identify possible fault lineations on the basis of bathymetry and seismicity. Arrows denote relative plate motion directions [*DeMets and Stein*, 1991]. See Figure 4 for further details.

the Menard (Figure 9) transforms may also be associated with extensional offsets.

At the western ridge-transform intersection of the Rivera transform, a normal-faulting earthquake and several strike-slip events with anomalously striking fault planes have occurred (Figure 10). Earthquake epicenters appear offset to the northeast of the expected transform location, although the constraint on locations in the direction perpendicular to the transform is weak. An extensional offset of the Rivera transform may occur west of 109°W. Alternatively, the earthquakes with anomalous mechanisms may reflect internal deformation of the Rivera plate.

Fox and Gallo [1984] argue that higher strain rates and the juxtaposition of thinner lithosphere will allow relay zones to develop more easily along transforms at fast spreading ridges. In accord with this hypothesis, extensional relay zones have been mapped along a number of other transforms along the East Pacific Rise, including the Tamayo [*Macdonald et al.*, 1979], the Orozco [*Tréhu and Solomon*, 1983; *Madsen et al.*, 1986], the Clipperton [*Gallo et al.*, 1986], and the Siqueiros [*Fornari et al.*, 1989] transforms, and the Quebrada, Discovery, Gofar, Wilkes, and Garrett transforms on the Pacific-Nazca spreading center [*Lonsdale*, 1989]. (A recent compilation of transforms known to

have extensional relay zones is given by *Fornari et al.* [1989].) The CMT catalogue does not include events with normal-faulting mechanisms along these transforms. An anomalous strike-slip earthquake, having a sense of slip opposite to that expected for transform motion, occurred along the right-stepping Gofar transform (Table 2), but this earthquake is probably associated with one of two small left-stepping offsets south of the Gofar [*Lonsdale*, 1989].

The lack of teleseismically observable normal-faulting earthquakes along most of the fastest slipping transforms may be because many of these extensional relay zones occur as intratransform spreading centers. At fast spreading rates, such relays would not be expected to display significant seismicity at teleseismic distances. Crustal thinning and magmatic activity (either intrusive or extrusive) within the extending region of the transform could yield anomalously high temperatures, at most a thin seismogenic layer, and thus a paucity of observable activity. The presence of amphibolite-facies metamorphic rocks collected in the vicinity of the pull-apart at 125.7°W on the Heezen transform provides indirect evidence for limited magmatic intrusion associated with crustal thinning [*Lonsdale*, 1986].

Extensional offsets may also have an influence on the rate of release of seismic moment along fast slipping transforms. The maximum moment of transform earthquakes appears to decrease and the moment rate deficit increases with increasing spreading rate [*Burr and Solomon*, 1978; *Kawasaki et al.*, 1985]. The presence of fault offsets could inhibit rupture of long fault segments and limit the maximum moments of earthquakes, although it is not clear how fault offsets would affect the total moment release. The thermal and compositional effects of offsets could also be important.

Influence of Changes in Spreading Direction

Changes in plate motion may lead to the occurrence of earthquakes with anomalous mechanisms by altering fault geometry and by introducing a component of compression or extension along the fault. For instance, along the Pacific-Nazca plate boundary, a recent small clockwise rotation is inferred to have created intratransform spreading centers within large-offset, right-stepping transforms [*Lonsdale*, 1989]. Others have suggested that recent plate motion changes have occurred along the Rivera, Eltanin, and St. Paul's transforms [*Lonsdale*, 1986; *DeMets and Stein*, 1990; *J.-G. Schilling*, unpublished cruise report, 1987]. We examine whether these changes appear to have been a significant influence in the occurrence of earthquakes with anomalous mechanisms and locations.

The Pacific-Rivera magnetic lineations show that the rise crest has progressively rotated 5–15° in a clockwise direction in the last 5 m.y. [*DeMets and Stein*, 1990], putting the left-stepping Rivera transform in compression. This change in spreading direction is compatible with the apparent rotation of stresses toward transform-perpendicular compression inferred from the anomalous strike-slip earthquakes near the ridge-transform intersection. Such a change would tend to destroy extensional relay zones along the left-stepping transform, although at least one such relay zone has been suggested on the basis of seismicity and bathymetry.

Recent plate motion changes at the Eltanin may explain the occurrence of several earthquakes with normal-faulting mechanisms. Magnetic anomalies north of the Heezen transform show a 10° clockwise rotation of spreading in the past 4 m.y., which would put the right-stepping transform in extension in the

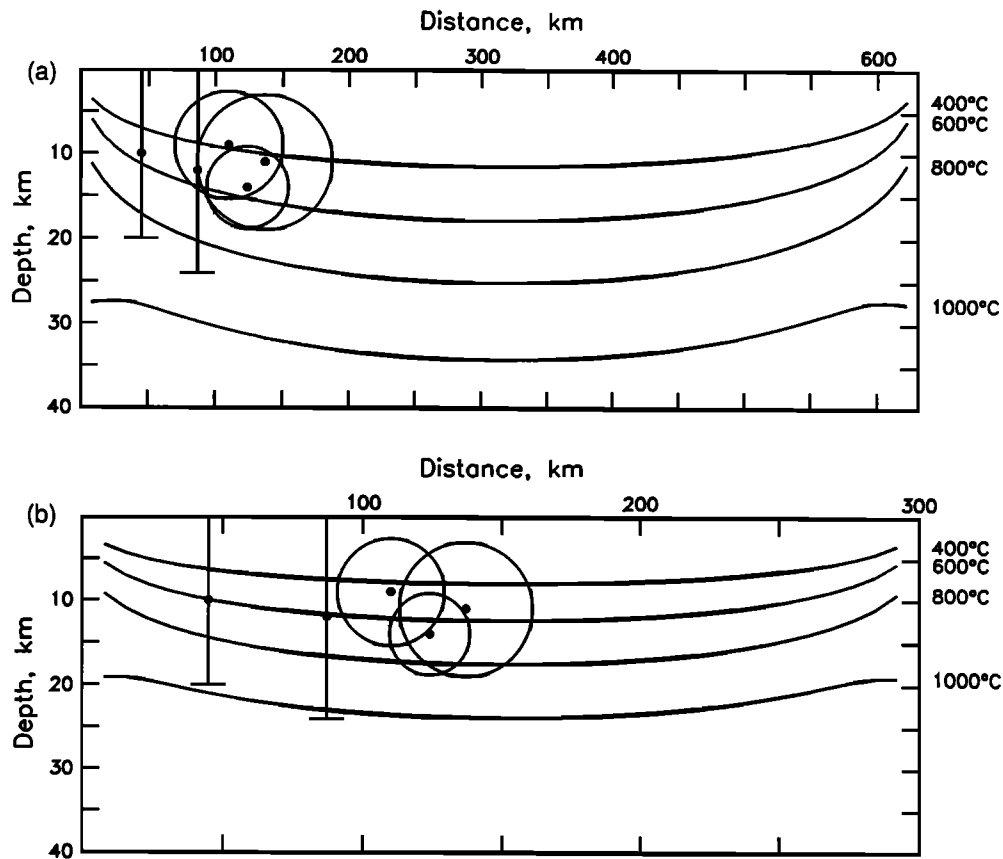


Figure 11. Centroid depths of earthquakes along the St. Paul's transform. (a) Thermal model derived for an offset of 630 km and an age difference of 39 Ma. (b) Thermal model derived for an offset of 300 km and an age difference of 19 Ma. Circles denote the areal extent of faulting for a circular fault model. Vertical bars denote a depth extent of faulting that is twice the centroid depth. See text for further details.

more recent past and would favor the development of extensional offsets [Lonsdale, 1986], similar to the situation along the Pacific-Nazca plate boundary.

The normal-faulting mechanisms along the Eltanin fault system and at the Menard transform may also reflect regional stresses caused by plate motion changes. Minor internal plate deformation in the past 20 m.y. near this region of the Pacific-Antarctic plate boundary has been suggested to explain the possible mismatch of fracture zones from plate reconstructions [Stock *et al.*, 1991]. Analysis of bathymetric and magnetic data [Molnar *et al.*, 1975; Lonsdale, 1986] and of geoid data [Mayes *et al.*, 1990] demonstrates the evolution of spreading direction in the past: the spacing between the Heezen and Tharp fracture zones decreased by 100 km due to changes in the spreading direction along the Pacific-Antarctic spreading center about 20-35 m.y. ago. The destruction of small, left-offsetting fracture zones and the creation of many small, right-offsetting fracture zones occurred during this counterclockwise change in plate motion [Molnar *et al.*, 1975], consistent with the view that transforms, particularly along fast spreading rises, are zones of weakness that can adjust readily during plate motion changes [Menard and Atwater, 1968]. Regional deformation may explain the occurrence of normal-faulting earthquakes with similar orientation both along the transforms and in intraplate settings, such as south of the Tharp transform.

A survey of the Mid-Atlantic Ridge north of the St. Paul's transform [Schilling *et al.*, 1987; J.-G. Schilling, unpublished

cruise report, 1987] revealed that the morphologic grain changed orientation from about N340-350°E to 0° over the past 0.2 My and that the ridge has propagated northward from the transform, perhaps in response to a clockwise change in spreading direction and rotation of the fracture zone, as proposed by Bonatti and Crane [1982] for the Vema transform. The change in ridge orientation may explain the ridge-perpendicular compressive stresses indicated by earthquakes with unusual mechanisms near the western ridge-transform intersection. J.-G. Schilling (unpublished cruise report, 1987) has suggested that this clockwise change in orientation may have led to the development of extensional relay zones in the transform.

In summary, there is some indication that changes in plate motion are responsible for the occurrence of anomalous earthquake activity along some oceanic transforms, but further evidence is required to support this hypothesis.

Thermal Stresses

Thermal stresses generated by the differential cooling of oceanic lithosphere have been suggested as a primary cause of oceanic intraplate earthquakes on the basis of the pattern of earthquake source characteristics with depth and seafloor age [Bratt *et al.*, 1985; Parmentier and Haxby, 1986]. Two-dimensional models of thermal stresses predict large, ridge-parallel extensional stresses near the ridge-transform intersection [Sandwell, 1986; Haxby and Parmentier, 1988]. It has also been proposed that fracture zones

form in response to such ridge-parallel extension [Collette, 1974; Turcotte, 1974]. The presence of earthquakes with mechanisms indicating that the least compressive horizontal stress is ridge-parallel in the vicinity of the ridge-transform intersections of the St. Paul's and Marathon transforms is thus consistent with a controlling influence by thermal stresses. A quantitative analysis comparing a larger set of earthquake data with appropriate three-dimensional models of thermal stress near oceanic transforms is necessary to provide a rigorous test of this hypothesis.

Evidence for a Weak Fault

As noted earlier, some oceanic and continental transforms appear to act as zones of weakness, with low shear stresses on the fault and a horizontal principal stress oriented in a nearly fault-normal direction in the lithosphere adjacent to the fault [Zoback *et al.*, 1987; Mount and Suppe, 1987; Wilcock *et al.*, 1990]. In this section, we consider whether transform earthquakes with anomalous mechanisms provide additional evidence for the presence of a weak fault zone.

On the St. Paul's and Marathon transforms, shallow reverse-faulting events with ridge-parallel fault strikes occur near the ridge-transform intersections. A strike-slip event with an unusual orientation occurred near the site of the reverse-faulting event at the St. Paul's transform. The mechanisms of these earthquakes indicate transform-perpendicular extension near the ridge-transform intersection. Near St. Paul's Rocks, on the other hand, the reverse-faulting focal mechanisms imply that the horizontal stresses are rotated toward transform-perpendicular compression. Differences in fault geometry and structure may account for this difference in the ordering of principal stresses. In the area of the compressive fault jog at the Owen transform, an anomalous strike-slip earthquake indicating transform-perpendicular compression occurred as an aftershock to an earthquake with mechanism compatible with transform-parallel motion. At the Eltanin transform, several normal-faulting earthquakes show an orientation of stresses similar to that of a normal-faulting intraplate earthquake that occurred 100 km south of the Tharp transform (Figure 1) and thus are more likely a response to a regional stress field. Earthquakes with anomalous strike-slip mechanisms near the Rivera transform indicate a stress field tending toward transform-perpendicular compression.

We see no strong evidence in these data to support the view that oceanic transforms are generally weaker than the surrounding lithosphere on the basis of a systematic perturbation to the regional stress field. Neither do the observations invalidate this hypothesis, however. The mechanisms of the large anomalous earthquakes in this study appear to be dominated by factors other than a systematically reduced strength on the transform. We note that no anomalous large earthquakes were found on the Kane transform, where the microearthquake experiment of Wilcock *et al.* [1990] found several events within the transform valley indicative of extension perpendicular to the transform.

CONCLUSIONS

A number of large earthquakes with mechanisms or locations inconsistent with simple models have occurred near large-offset oceanic transform faults. Much of the anomalous earthquake activity can be associated with complex fault geometry or large structural features that apparently influence slip on the fault. Compressional fault jogs associated with anomalous structures are

likely responsible for earthquakes with unusual mechanisms on the Owen and St. Paul's transforms. A normal-faulting earthquake on the Heezen transform occurs at the edge of an extensional offset, and other normal-faulting earthquakes on transforms along the East-Pacific Rise may likewise be associated with extensional offsets.

Several other factors may contribute to the occurrence of such earthquakes, but we do not find strong evidence to support their influence. Recent changes in plate motion, suggested to have occurred at the Eltanin, Rivera, and St. Paul's transforms, could contribute to the presence of anomalous earthquakes by influencing fault geometry or the state of stress along the fault. Thermal stresses near ridge-transform intersections may lead to earthquakes having reverse-faulting mechanisms characterized by a ridge-parallel least compressive stress; events with such mechanisms are seen near the ridge-transform intersections of the St. Paul's and Marathon transforms. While some earthquakes show evidence for a nearly transform-perpendicular orientation of one of the principal horizontal stresses, consistent with a weak fault zone, our results do not resolve whether oceanic transforms are generally weaker than surrounding lithosphere.

APPENDIX: EARTHQUAKE SOURCE MECHANISMS FROM BODY WAVEFORM INVERSION

In this appendix we present the details of long-period *P* and *SH* waveform inversion for the 13 transform earthquakes listed in Table 1. The orientation (strike/dip/slip) of each double-couple mechanism is presented according to the convention of Aki and Richards [1980]. Centroid depths are given relative to the seafloor.

July 29, 1983, Owen Transform (Figure A1)

Waveform inversion for this event indicates a mechanism of 214/89/298, similar to the CMT solution of 37/71/44 [Dziwonski *et al.*, 1984], and consistent with either predominantly dip-slip motion on a nearly vertical fault oriented approximately parallel to the transform or primarily right-lateral strike-slip motion on a northeasterly dipping low-angle fault. Vertical short-period records at KEV and CHG were examined to confirm the polarity of the first pulses. The *SH* wave data for this event provide strong constraints on the unusual mechanism. The minimum residual occurs for centroid depths between 6 and 16 km.

July 7, 1986, Owen Transform (Figure A2)

The earthquake of July 7, 1986, on the Owen transform is the largest event ($M_0 = 3.7 \times 10^{25}$ dyn cm) in the catalogue of anomalous transform events. There is good coverage of the focal sphere, and the waveforms are best fit by a reverse-faulting solution (238/36/095) at a centroid depth of 4 km. This source mechanism is similar to the CMT solution of 242/42/098 [Dziwonski *et al.*, 1987b]. Solutions constrained to be shallower or deeper than 4 km have jagged source time functions and higher rms residual variances. *P* wave reverberations indicate a water depth of 4 km.

October 11, 1973, St. Paul's Transform (Figure A3)

On October 11, 1973, the ISC reported two events separated by approximately 10 s. The earlier, smaller event falls on the map trend of transform activity while the later, larger event occurred off-trend (Figure 4 and events 15 and 16 in Figure 3b). The unusual

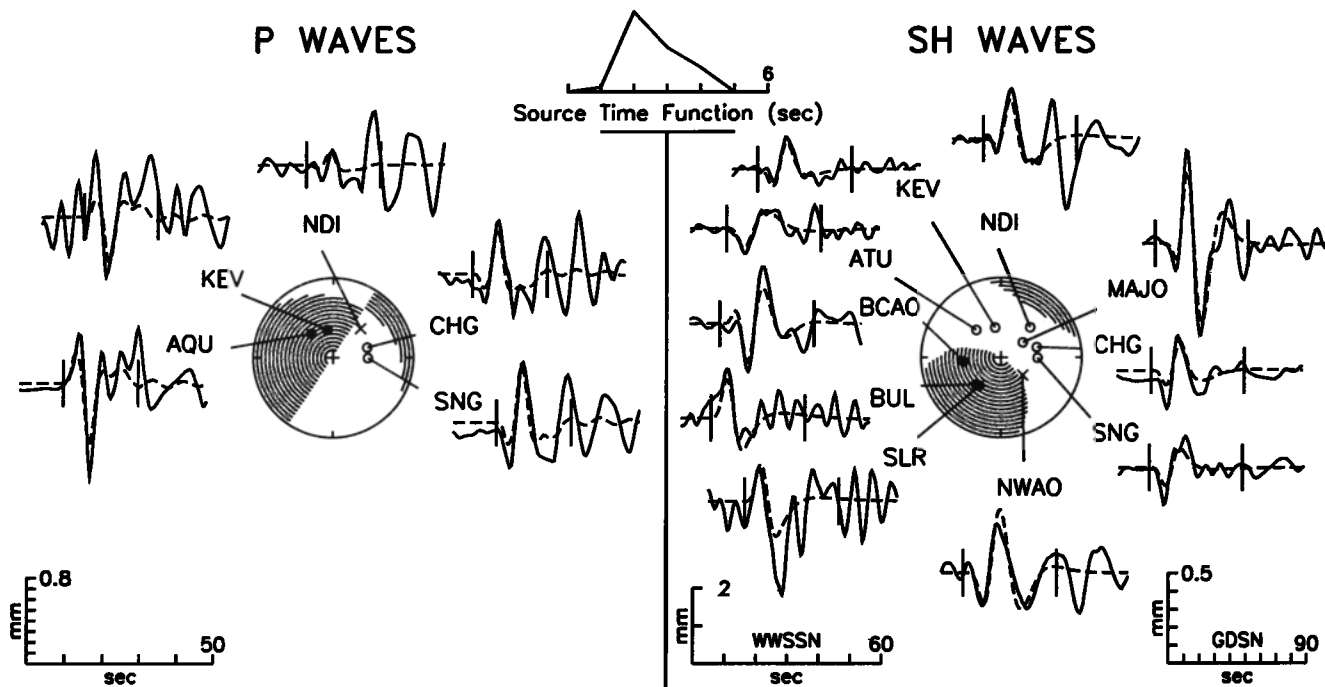


Fig. A1. Observed (solid curve) long-period *P* and *SH* waveforms from the earthquake of July 29, 1983, compared with synthetic waveforms (dashed curves) generated from the best fitting point source model found from body waveform inversion. Waveforms from GDSN stations (MAJO, NWAO, and BCAA) are plotted at the scale shown in the lower right. *P* and *SH* radiation patterns are shown on the lower focal hemisphere (equal-area projection). For *SH* waves, compression corresponds to positive motion as defined by *Aki and Richards* [1980]. All amplitudes are normalized to an epicentral distance of 40° and a WWSSN instrument magnification of 1500; the amplitude scales correspond to the waveforms that would be observed on an original seismogram from such an instrument. The two vertical lines show the portion of each time series used in the inversion. Open circles denote dilatational first motions, solid circles denote compressional first motions, and crosses denote emergent arrivals.

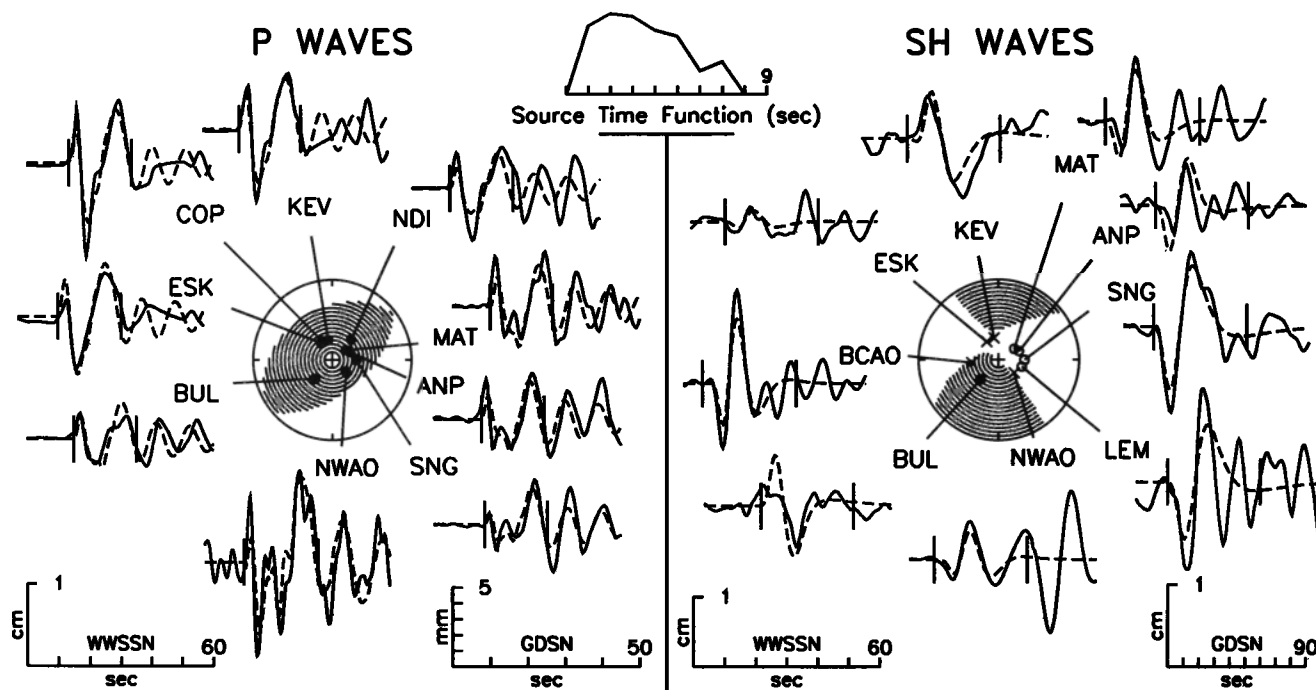


Fig. A2. Observed *P* and *SH* waveforms from the earthquake of July 7, 1986, compared with synthetic waveforms generated from the best fitting point source model found from body waveform inversion. See Figure A1 for further details.

character of these locations made body waveform analysis of these events desirable. For the smaller event, we could not resolve a mechanism, and we fixed the parameters to those of a conventional strike-slip event. For the larger event, we parameterized the STF as a horizontal rupture along the nodal plane striking at 264°. Minimization of the rms residual indicates a centroid depth in the range 9-15 km, consistent with apparent depth phases in *P* waves at ESK, IST, and JER.

November 14, 1982, St. Paul's Transform (Figure A4)

Our analysis shows that this earthquake involved almost purely strike-slip faulting, although the probable fault plane appears to depart from the vertical. This event is well fit by a simple STF at 9-13 km centroid depth. Our solution of 86/66/172 is in good agreement with the CMT solution of 85/90/180 [Dziewonski et al., 1983a].

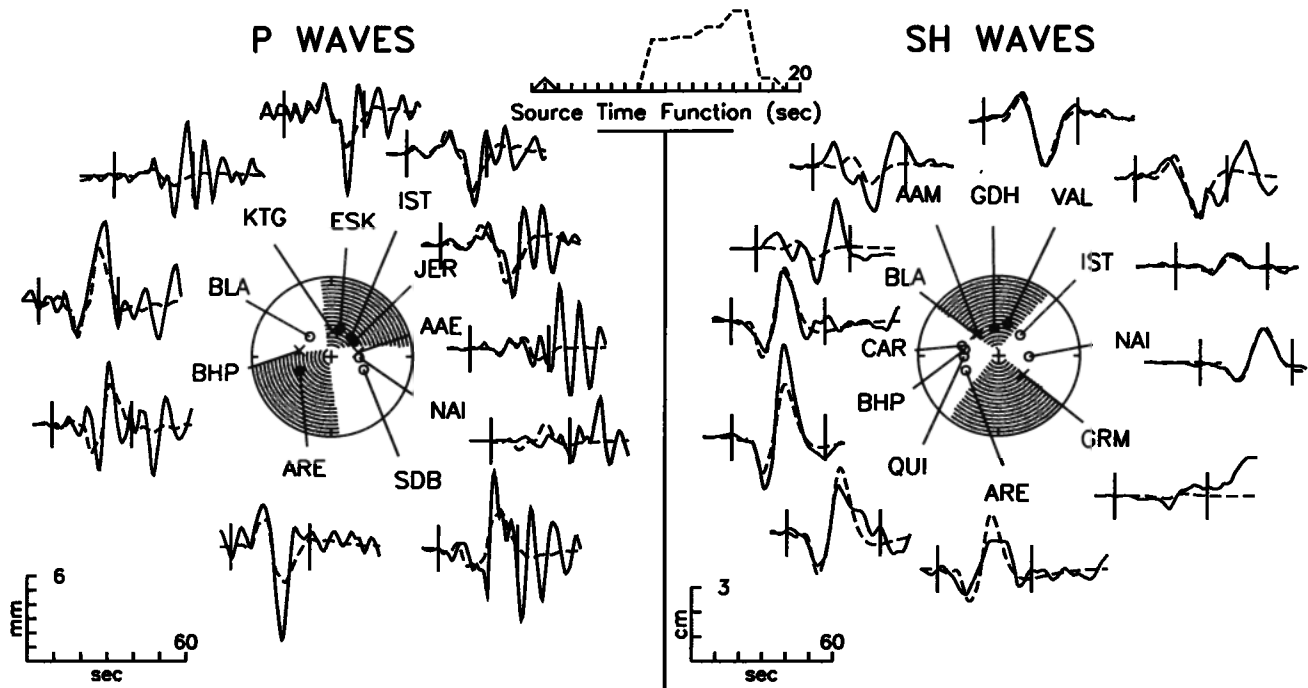


Fig. A3. Observed *P* and *SH* waves from the earthquake of October 11, 1973, compared with synthetic waveforms generated for a source model with two point sources. The parameters of the first, smaller, event were fixed in the inversion; the source parameters of the second event are found from body waveform inversion. The radiation pattern of the larger subevent is shown. See Figure A1 for further details.

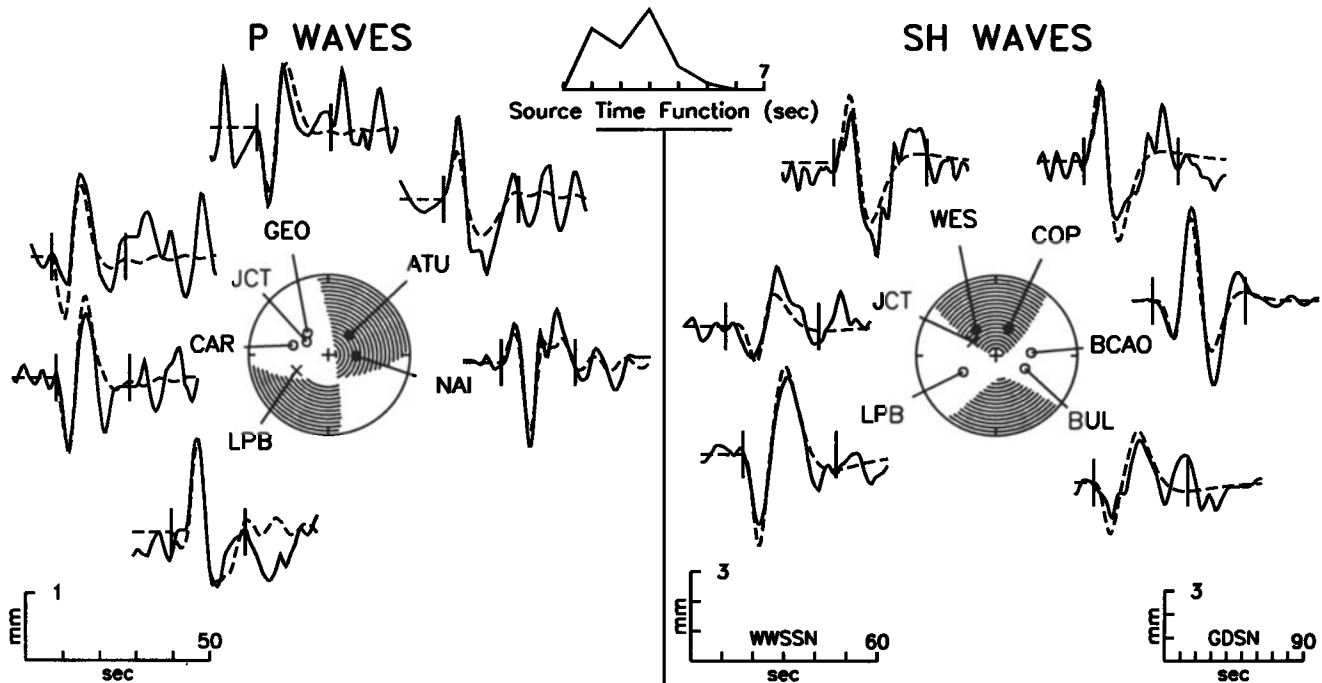


Fig. A4. Observed *P* and *SH* waves from the earthquake of November 14, 1982, compared with synthetic waveforms generated from the best fitting point source model found from body waveform inversion. See Figure A1 for further details.

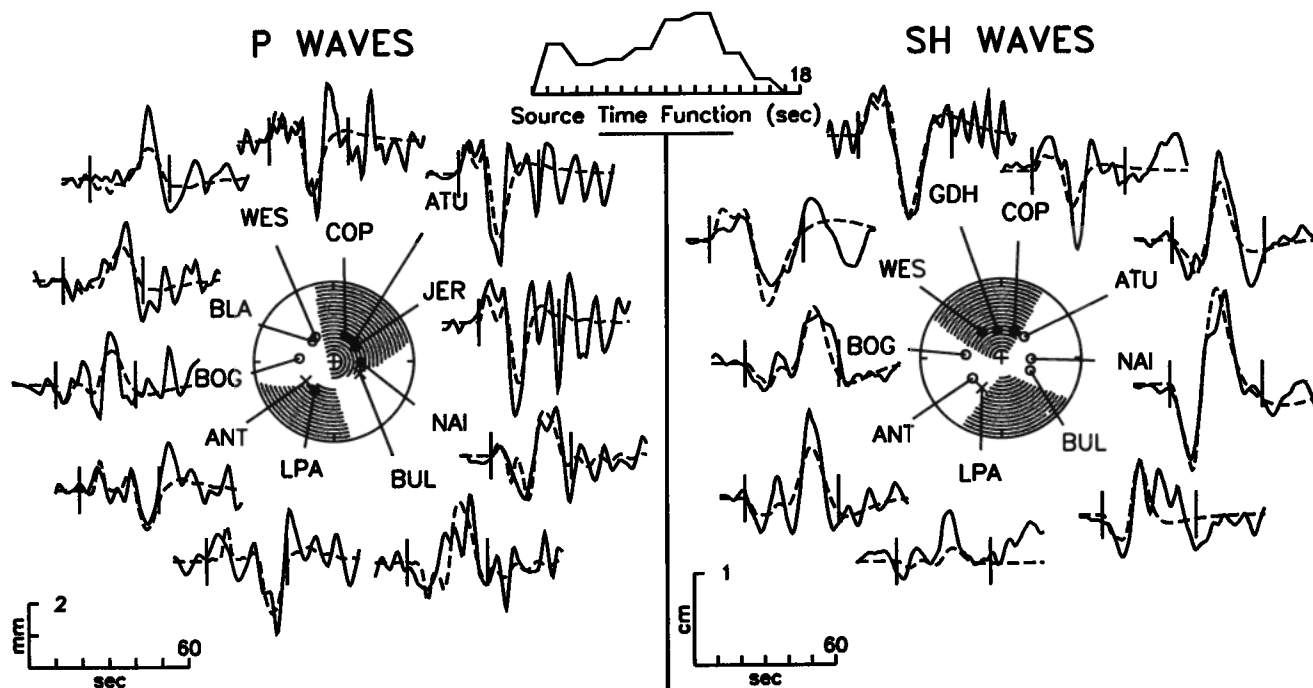


Fig. A5. Observed *P* and *SH* waveforms from the earthquake of October 12, 1985, compared with synthetic waveforms generated from the best fitting point source model found from body waveform inversion. See Figure A1 for further details.

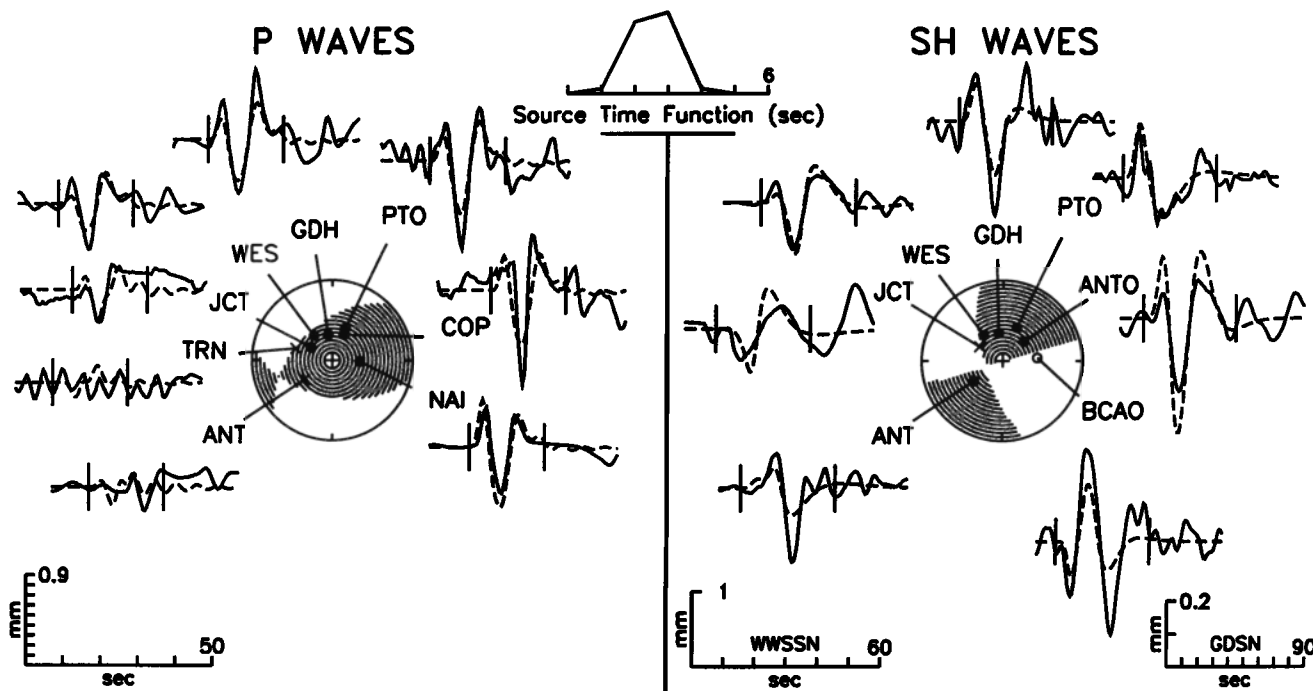


Fig. A6. Observed *P* and *SH* waveforms from the earthquake of September 20, 1986, compared with synthetic waveforms generated from the best fitting point source model found from body waveform inversion. ANTO is a GDSN station. See Figure A1 for further details.

October 12, 1985, St. Paul's Transform (Figure A5)

For this earthquake we parameterized the STF as a horizontal rupture along the nodal plane striking at 76°. Analysis of waveform data indicates a predominantly strike-slip mechanism. The minimum residual occurs at 7-13 km centroid depth. The STF length of 17 s is unusually long for an event of moment 4×10^{25}

dyn cm, and the relatively high level of low-frequency excitation indicated by free oscillation amplitudes indicates that this is a slow earthquake (T.H. Jordan, personal communication, 1991). Our mechanism solution of 76/72/174 is in good agreement with the CMT solution of 83/75/179 [Dziewonski et al. 1986b].

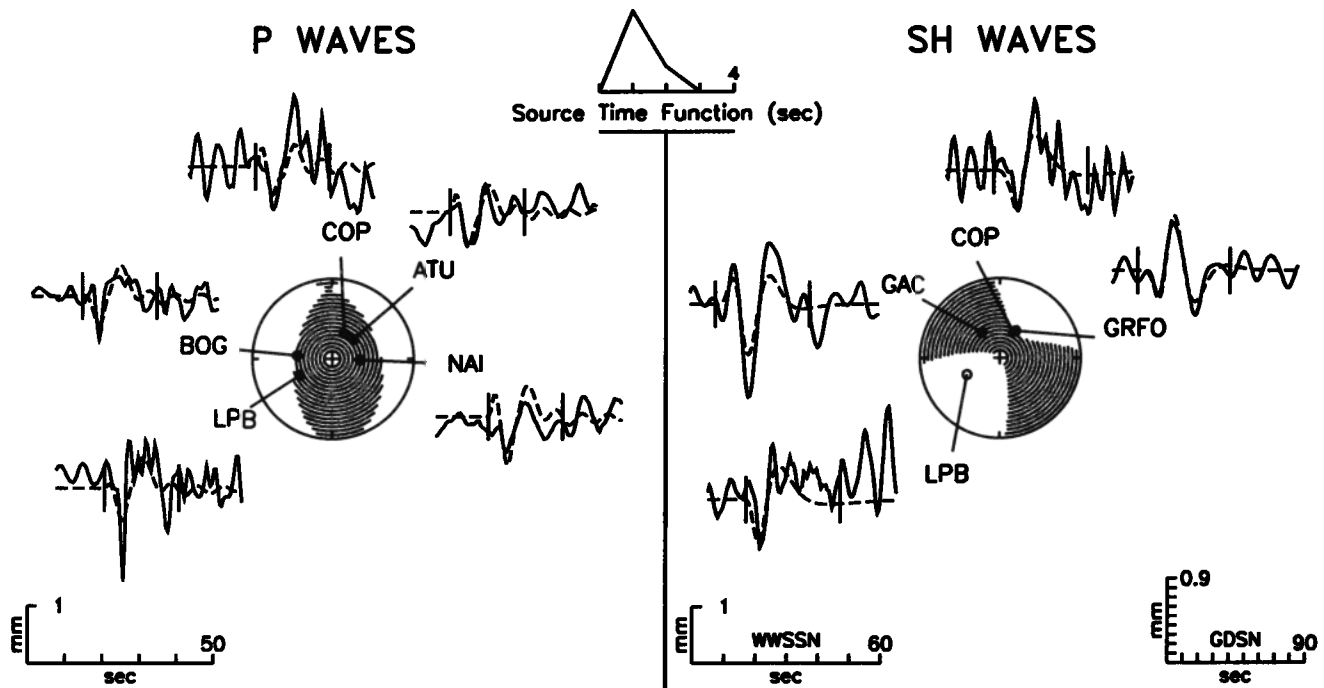


Fig. A7. Observed *P* and *SH* waveforms from the earthquake of April 20, 1988, compared with synthetic waveforms generated from the best fitting point source model found from body waveform inversion. GRFO is a GDSN station. See Figure A1 for further details.

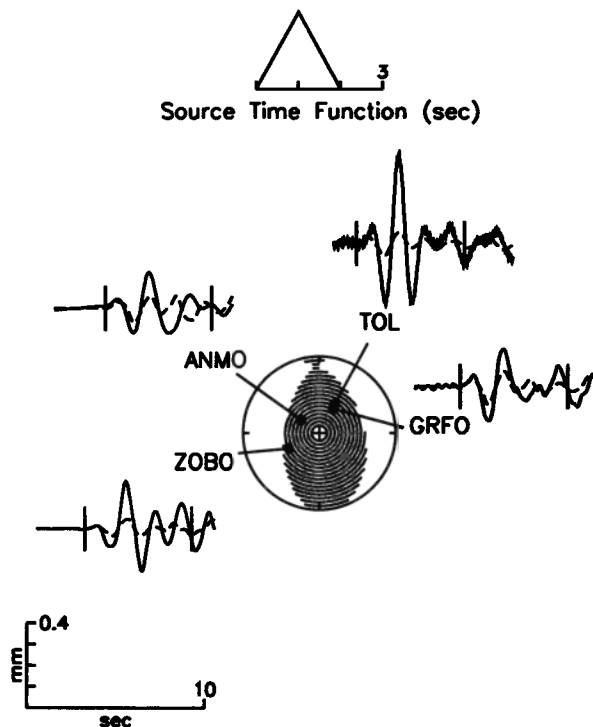


Fig. A8. Observed short-period *P* waveforms from the earthquake of April 20, 1988, compared with synthetic waveforms generated from the mechanism found from long-period body waveform inversion. All data are from GDSN stations. See Figure A1 for further details.

September 20, 1986, St. Paul's Transform (Figure A6)

Although this earthquake is located along the trend of principal seismic activity, a thrust mechanism (246/60/090) is reported in the

Harvard CMT catalogue [Dziewonski *et al.*, 1987b]. Despite the small moment of this event, we were able to obtain good *P* and *SH* coverage of the focal sphere. The mechanism (227/53/50) obtained from body waveform inversion contains a small strike-slip component; this strike-slip motion is in the expected direction for transform slip if the southward dipping nodal plane is the fault plane. The overall fit as described by the rms residual displays a distinct minimum over the centroid depth range 12-16 km.

April 20, 1988, St. Paul's Transform (Figures A7 and A8)

Our reverse-faulting solution of 189/52/107 differs somewhat from the CMT solution of 196/78/108 [Dziewonski *et al.*, 1989b], which has a steeper dip. The discrepancy may be attributed to the poor signal-to-noise ratio for this small event. The identification of the first pulse is ambiguous in the long-period *P* wave data (Figure A7), but compressional first motions, consistent with a thrust mechanism, are confirmed in the vertical short-period waveforms (Figure A8). For the short-period *P* wave synthetics, a value of 0.6 s is taken for t^* , and the mechanism is that from long-period waveform inversion. A centroid depth of 8 km is required by long-period data and also provides a good fit to the short-period data. Water reverberations indicate a seafloor depth of about 2.5 km.

December 23, 1988, St. Paul's Transform (Figure A9)

The Harvard CMT catalogue lists a reverse-faulting mechanism of 245/57/094 for this earthquake [Dziewonski *et al.*, 1989c]. Inversion of body waveforms from WWSSN records indicates a mechanism of 228/56/072, a similarly reverse-faulting solution but with different strike and slip angles from the CMT solution. Our preferred centroid depth is in the range of 7-11 km, on the basis of both the residual variance and the observed fit to the waveforms. The small first *SH* arrivals at WES and BLA provide constraints on the strike of the source mechanism.

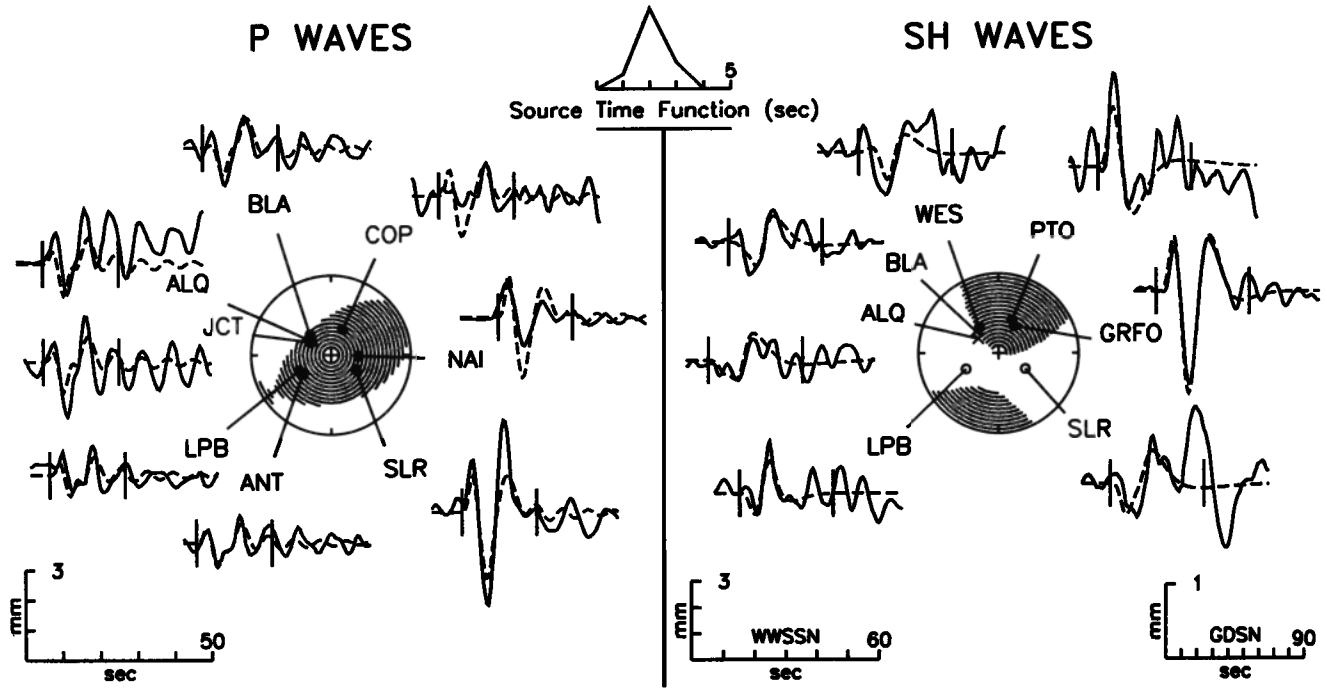


Fig. A9. Observed *P* and *SH* waveforms from the earthquake of December 23, 1988, compared with synthetic waveforms generated from the best fitting point source model found from body waveform inversion. See Figure A1 for further details.

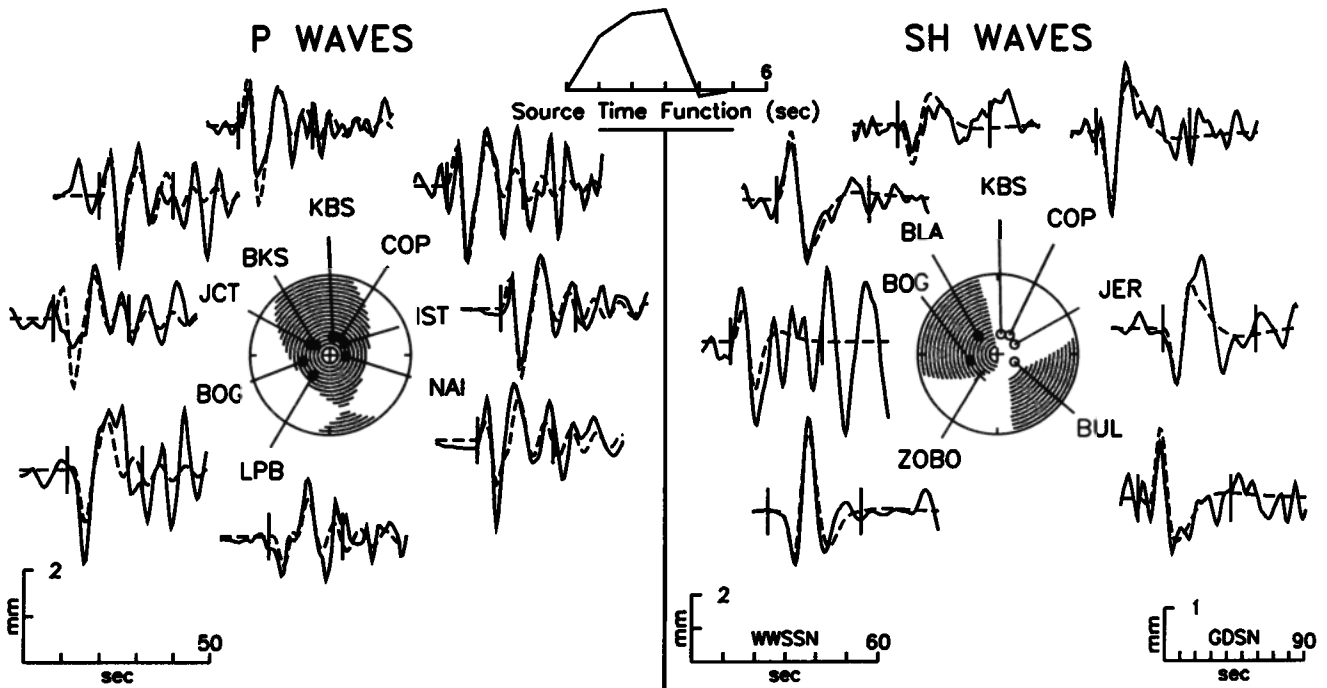


Fig. A10. Observed *P* and *SH* waveforms from the earthquake of September 22, 1985, compared with synthetic waveforms generated from the best fitting point source model found from body waveform inversion. ZOBO is a GDSN station. See Figure A1 for further details.

September 9, 1985, Marathon Transform (Figure A10)

Our mechanism solution for this event is 140/54/051, corresponding to primarily reverse faulting on a fault oblique or orthogonal to the transform. The CMT reverse-faulting solution is 196/31/111 [Dziewonski et al, 1986a]. The polarity was found to be reversed on ZOBO (*SH*). This is a well-fit shallow event, with

a centroid depth of 3-5 km, as required by a minimization of the rms residual.

February 17, 1978, Heezen Transform (Figure A11)

Although coverage is sparse and the signal-to-noise ratio is low, the combination of both *P* and *S* waveforms suggests a mechanism

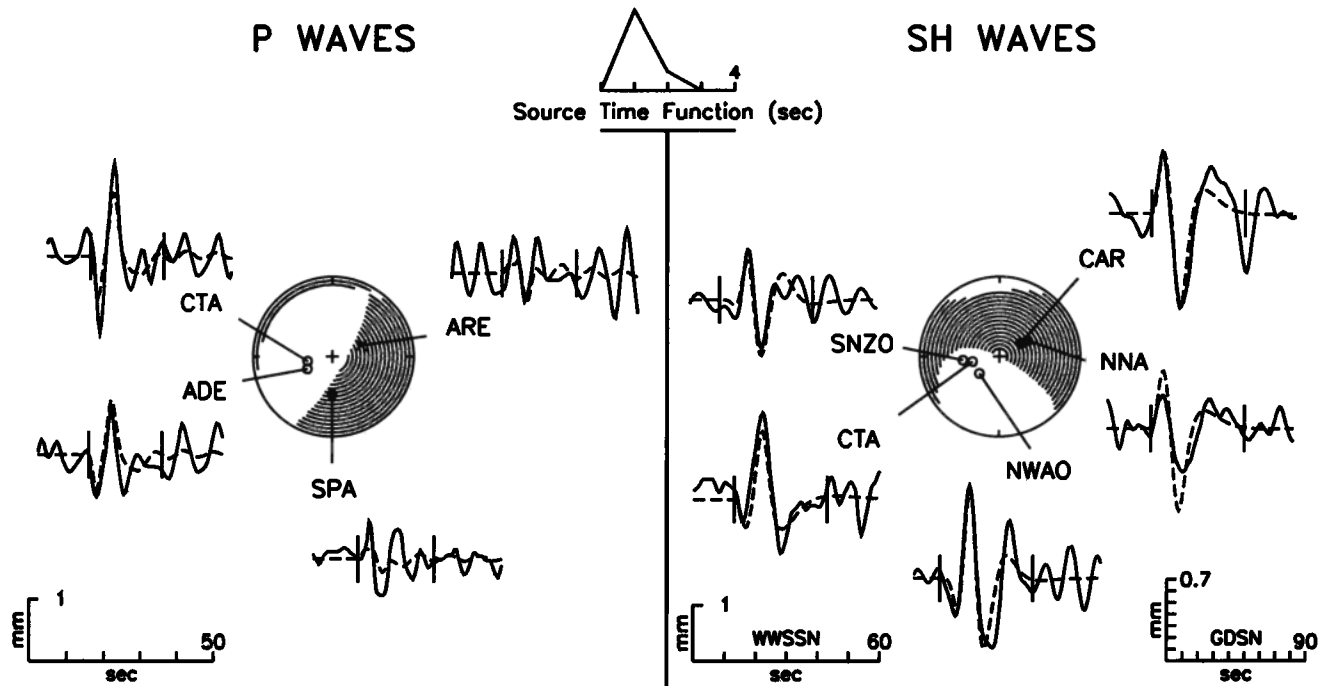


Fig. A11. Observed *P* and *SH* waveforms from the earthquake of February 17, 1978, compared with synthetic waveforms generated from the best fitting point source model found from body waveform inversion. SNZO is a GDSN station. See Figure A1 for further details.

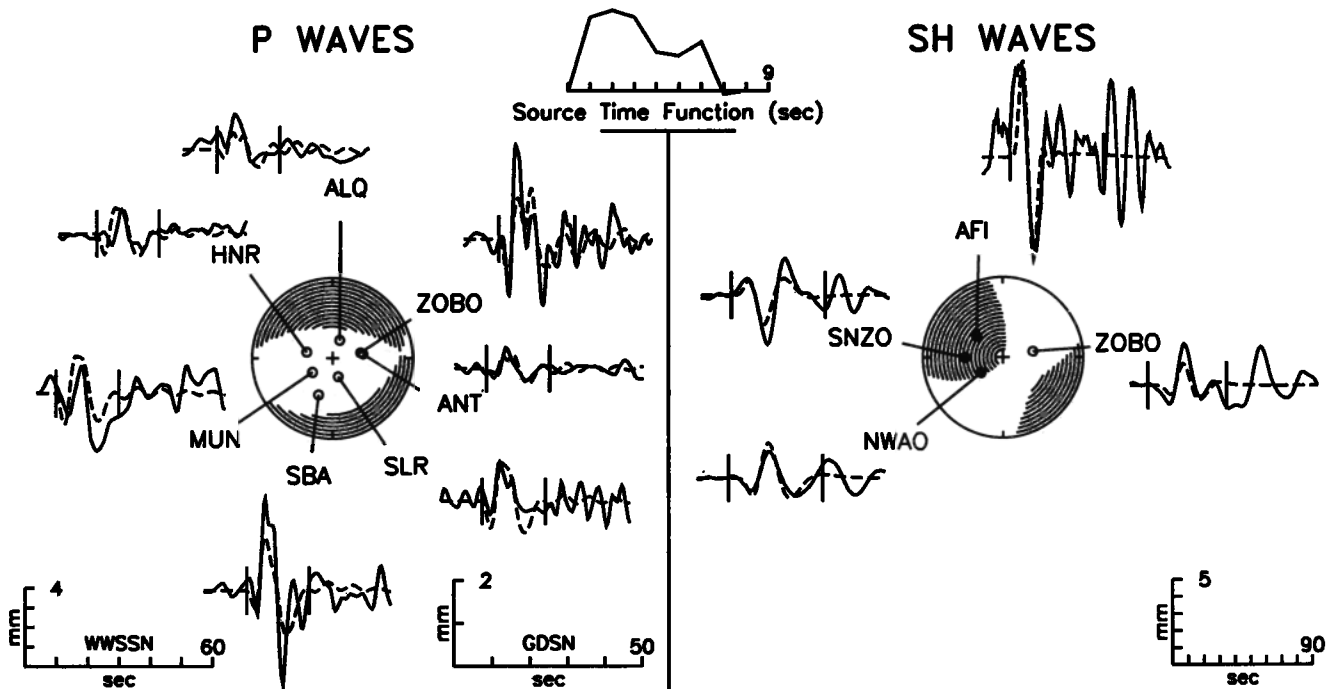


Fig. A12. Observed *P* and *SH* waveforms from the earthquake of May 27, 1989, compared with synthetic waveforms generated from the best fitting point source model found from body waveform inversion. AFI is a GDSN station. See Figure A1 for further details.

of 241/16/301, which has a smaller dip and a larger strike-slip component than the CMT mechanism of 256/34/287 [Dziewonski *et al.*, 1987c]. The best fitting centroid depth ranges from 8 to 14 km, but *P* wave coverage is poor. The predicted polarity of *P* wave first motions is in agreement with short-period records.

May 27, 1989, Tharp Transform (Figure A12)

Our normal-faulting solution of 275/59/287 is similar to the CMT mechanism of 258/57/277 [Dziewonski *et al.*, 1990b]. Examination of short-period records shows that this event has a

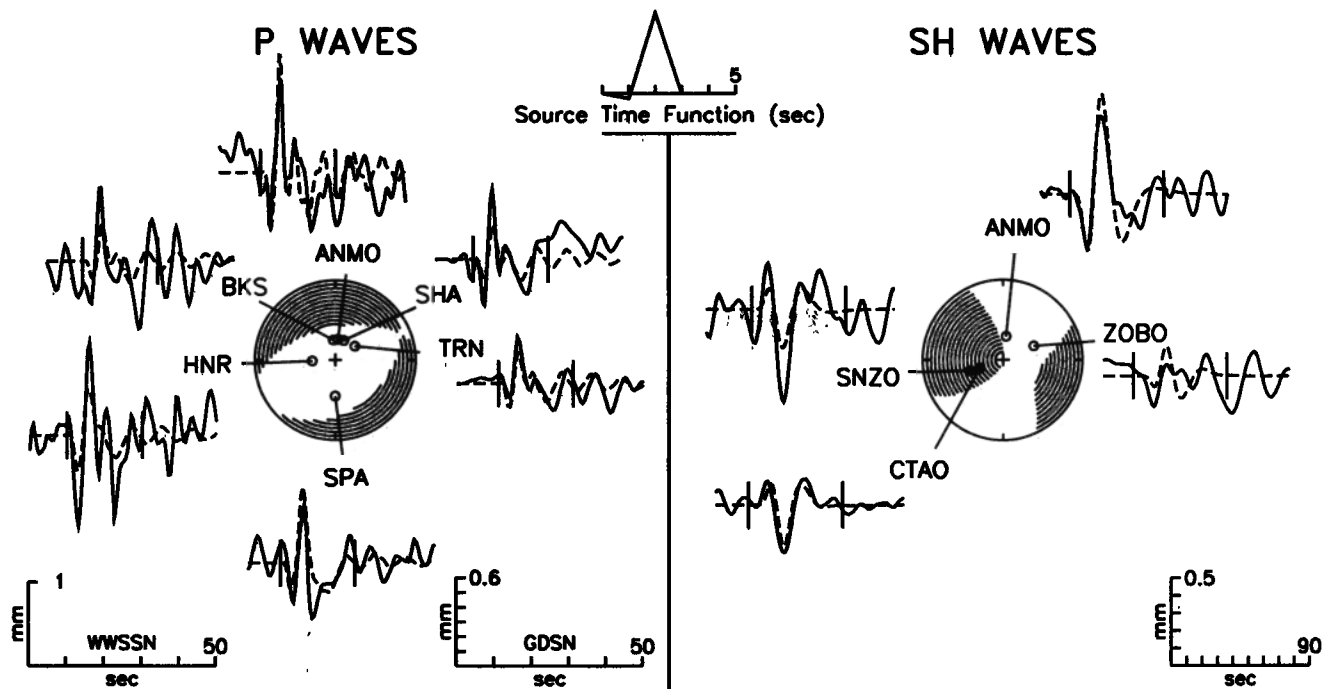


Fig. A13. Observed *P* and *SH* waveforms from the earthquake of May 15, 1987, compared with synthetic waveforms generated from the best fitting point source model found from body waveform inversion. CTAO and ANMO are GDSN stations. See Figure A1 for further details.

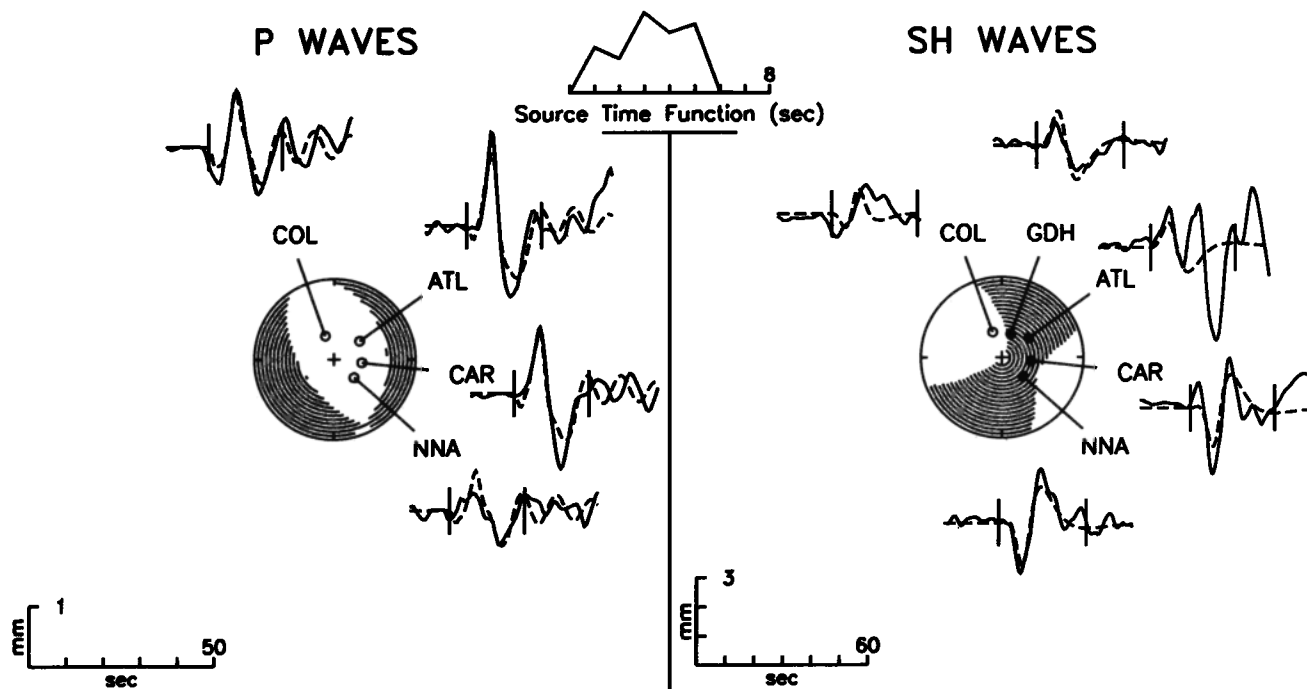


Fig. A14. Observed *P* and *SH* waveforms from the earthquake of September 21, 1977, compared with synthetic waveforms generated from the best fitting point source model found from body waveform inversion. See Figure A1 for further details.

precursor that is not evident in the long-period records, although there are high noise levels on long-period records prior to the onset of the *P* wave of the main event. Our best fitting centroid depth is approximately 10 km, but the *P* wave signal-to-noise ratio is poor.

May 15, 1987, Menard Transform (Figure A13)

We find a normal-faulting mechanism of 50/37/247, in agreement with the CMT solution of 53/37/260 [Dziewonski *et al.*,

1988*b*]. The dilatational first motions are confirmed by examination of short-period vertical records. Centroid depth is within the range 7-11 km, but the *P* wave signal-to-noise ratio is low.

September 21, 1977, Rivera Transform (Figure A14)

We find a normal-faulting mechanism of 353/35/291. The CMT mechanism is 346/72/254 [Dziewonski *et al.*, 1987*a*]. The

preferred centroid depth is 4 km, but the *P* wave signal-to-noise ratio is low.

Acknowledgements. We thank Jim Cochran, Peter Hunter, Peter Lonsdale, and Jean-Guy Schilling for providing survey data for individual transforms. We also thank Geoff Abers, Göran Ekström, Tom Jordan, and Bob Woodward for helpful information and Marcia McNutt for contributing support for this project. Jian Lin, Aristeo Pelayo, and Anne Tréhu provided constructive reviews. This research was supported by the National Science Foundation under grant EAR-9004750 and the National Aeronautics and Space Administration under grants NAG5-1921 and NAG5-2206.

REFERENCES

- Aki, K., and P. G. Richards, *Quantitative Seismology: Theory and Methods*, vol. 1, p. 114, W.H. Freeman, New York, 1980.
- Anderson, E. M., *The Dynamics of Faulting and Dyke Formation With Applications to Britain*, 2nd ed., 206 pp., Oliver and Boyd, Edinburgh, 1951.
- Anderson, R. S., Evolution of the northern Santa Cruz Mountains by advection of crust past a San Andreas fault bend, *Science*, 249, 397-401, 1990.
- Barka, A. A., and K. Kadinsky-Cade, Strike-slip fault geometry in Turkey and its influence on earthquake activity, *Tectonics*, 7, 663-684, 1988.
- Bergman, E. A., and S. C. Solomon, Transform fault earthquakes in the North Atlantic: Source mechanisms and depth of faulting, *J. Geophys. Res.*, 93, 9027-9057, 1988.
- Bergman, E. A., and S. C. Solomon, Earthquake swarms on the Mid-Atlantic Ridge: Products of magmatism or extensional tectonics?, *J. Geophys. Res.*, 95, 4943-4965, 1990.
- Bergman, E. A., J.L. Nabelek, and S. C. Solomon, An extensive region of off-ridge normal-faulting earthquakes in the southern Indian Ocean, *J. Geophys. Res.*, 89, 2425-2443, 1984.
- Bilham, R., and G. King, The morphology of strike-slip faults: Examples from the San Andreas fault, California, *J. Geophys. Res.*, 94, 10,204-10,216, 1989.
- Bonatti, E., Vertical tectonism in oceanic fracture zones, *Earth Planet. Sci. Lett.*, 37, 369-379, 1978.
- Bonatti, E., Subcontinental mantle exposed in the Atlantic Ocean on St. Peter-Paul islets, *Nature*, 345, 800-802, 1990.
- Bonatti, E., and K. Crane, Oscillatory spreading explanation of anomalously old uplifted crust near oceanic transforms, *Nature*, 300, 343-345, 1982.
- Bonatti, E., and P. R. Hamlyn, Mantle uplifted block in the western Indian Ocean, *Science*, 201, 249-251, 1978.
- Bowen, A. N., and R. S. White, Deep-tow seismic profiles from the Vema transform and ridge-transform intersection, *J. Geol. Soc. London*, 143, 807-817, 1986.
- Bratt, S. R., E. A. Bergman, and S.C. Solomon, Thermoelastic stress: How important as a cause of earthquakes in young oceanic lithosphere?, *J. Geophys. Res.*, 90, 10,249-10,260, 1985.
- Brune, J. N., T. L. Henyey, and R. F. Roy, Heat flow, stress, and rate of slip along the San Andreas fault, California, *J. Geophys. Res.*, 74, 3821-3827, 1969.
- Burr, N. C., and S. C. Solomon, The relationship of source parameters of oceanic transform earthquakes to plate velocity and transform length, *J. Geophys. Res.*, 83, 1193-1205, 1978.
- Byerlee, J., Friction of rocks, *Pure Appl. Geophys.*, 116, 615-626, 1978.
- Cochran, J. R., The Gulf of Aden: Structure and evolution of a young ocean basin and continental margin, *J. Geophys. Res.*, 86, 263-287, 1981.
- Cochran, J. R., Somali Basin, Chain Ridge, and origin of the northern Somali Basin gravity and geoid low, *J. Geophys. Res.*, 93, 11,985-12,008, 1988.
- Collette, B. J., Thermal contraction joints in a spreading seafloor as origin of fracture zones, *Nature*, 251, 299-300, 1974.
- Collette, B. J., A. P. Slootweg, and W. Twigt, Mid-Atlantic Ridge crest topography between 12° and 15° N, *Earth Planet. Sci. Lett.*, 42, 103-108, 1979.
- Collette, B. J., J. Verhoef, and A. F. J. de Mulder, Gravity and a model of the median valley, *J. Geophys.*, 47, 91-98, 1980.
- Collette, B. J., A. P. Slootweg, J. Verhoef, and W. R. Roest, Geophysical investigations of the floor of the Atlantic Ocean between 10° and 38°N (Kroonvlag-project), *Proc. K. Ned. Akad. Wet., Ser. B*, 87, 1-76, 1984.
- Dauphin, J. P., and G. E. Ness, Bathymetry of the gulf and peninsular province of the Californias, *AAPG Mem.*, 47, 21-23, 1991.
- DeMets, C., and S. Stein, Present-day kinematics of the Rivera plate and implications for tectonics in southwestern Mexico, *J. Geophys. Res.*, 95, 21,931-21,948, 1990.
- DeMets, C., R. G. Gordon, D. F. Argus, and S. Stein, Current plate motions, *Geophys. J. Int.*, 101, 425-478, 1990.
- Dziewonski, A. M., and J. H. Woodhouse, An experiment in systematic study of global seismicity: Centroid-moment tensor solutions for 201 moderate and large earthquakes in 1981, *J. Geophys. Res.*, 88, 3247-3271, 1983.
- Dziewonski, A. M., T. A. Chou, and J. H. Woodhouse, Determination of earthquake source parameters from waveform data for studies of global and regional seismicity, *J. Geophys. Res.*, 86, 2825-2852, 1981.
- Dziewonski, A. M., A. Friedman, D. Giardini, and J. H. Woodhouse, Global seismicity of 1982: Centroid-moment tensor solutions for 308 earthquakes, *Phys. Earth Planet. Inter.*, 33, 76-90, 1983a.
- Dziewonski, A. M., J. E. Franzen, and J. H. Woodhouse, Centroid-moment tensor solutions for April-June 1983, *Phys. Earth Planet. Inter.*, 33, 243-249, 1983b.
- Dziewonski, A. M., J. E. Franzen, and J. H. Woodhouse, Centroid-moment tensor solutions for July-September 1984, *Phys. Earth Planet. Inter.*, 34, 1-8, 1984.
- Dziewonski, A. M., J. E. Franzen, and J. H. Woodhouse, Centroid-moment tensor solutions for October-December 1984, *Phys. Earth Planet. Inter.*, 39, 147-156, 1985.
- Dziewonski, A. M., J. E. Franzen, and J. H. Woodhouse, Centroid-moment tensor solutions for July-September 1985, *Phys. Earth Planet. Inter.*, 42, 205-214, 1986a.
- Dziewonski, A. M., J. E. Franzen, and J. H. Woodhouse, Centroid-moment tensor solutions for October-December 1985, *Phys. Earth Planet. Inter.*, 43, 185-195, 1986b.
- Dziewonski, A. M., G. Ekström, J. E. Franzen, and J. H. Woodhouse, Global seismicity of 1977: Centroid-moment tensor solutions for 471 earthquakes, *Phys. Earth Planet. Inter.*, 45, 11-36, 1987a.
- Dziewonski, A. M., G. Ekström, J. E. Franzen, and J. H. Woodhouse, Centroid-moment tensor solutions for July-September 1986, *Phys. Earth Planet. Inter.*, 46, 305-315, 1987b.
- Dziewonski, A. M., G. Ekström, J. E. Franzen, and J. H. Woodhouse, Global seismicity of 1978: Centroid-moment tensor solutions for 512 earthquakes, *Phys. Earth Planet. Inter.*, 46, 316-342, 1987c.
- Dziewonski, A. M., G. Ekström, J. E. Franzen, and J. H. Woodhouse, Global seismicity of 1980: Centroid-moment tensor solutions for 515 earthquakes, *Phys. Earth Planet. Inter.*, 50, 127-154, 1988a.
- Dziewonski, A. M., G. Ekström, J. H. Woodhouse, and G. Zwart, Centroid-moment tensor solutions for April-June 1987, *Phys. Earth Planet. Inter.*, 50, 215-225, 1988b.
- Dziewonski, A. M., G. Ekström, J. E. Franzen, and J. H. Woodhouse, Global seismicity of 1982 and 1983: Additional centroid-moment tensor solutions for 553 earthquakes, *Phys. Earth Planet. Inter.*, 53, 17-45, 1988c.
- Dziewonski, A. M., G. Ekström, J. H. Woodhouse, and G. Zwart, Centroid-moment tensor solutions for October-December 1987, *Phys. Earth Planet. Inter.*, 54, 10-21, 1989a.
- Dziewonski, A. M., G. Ekström, J. H. Woodhouse, and G. Zwart, Centroid-moment tensor solutions for April-June 1988, *Phys. Earth Planet. Inter.*, 54, 199-209, 1989b.
- Dziewonski, A. M., G. Ekström, J. H. Woodhouse, and G. Zwart, Centroid-moment tensor solutions for October-December 1988, *Phys. Earth Planet. Inter.*, 57, 179-191, 1989c.
- Dziewonski, A. M., G. Ekström, J. H. Woodhouse, and G. Zwart, Centroid-moment tensor solutions for January-March 1989, *Phys. Earth Planet. Inter.*, 59, 233-242, 1990a.
- Dziewonski, A. M., G. Ekström, J. H. Woodhouse, and G. Zwart, Centroid-moment tensor solutions for April-June 1989, *Phys. Earth Planet. Inter.*, 60, 243-253, 1990b.
- Dziewonski, A. M., G. Ekström, J. H. Woodhouse, and G. Zwart, Centroid-moment tensor solutions for October-December 1989, *Phys. Earth Planet. Inter.*, 62, 194-207, 1990c.
- Dziewonski, A. M., G. Ekström, J. H. Woodhouse, and G. Zwart, Centroid-moment tensor solutions for October-December 1990, *Phys. Earth Planet. Inter.*, 68, 201-204, 1991.
- Ebel, J. E., L. J. Burdick, and G. S. Stewart, The source mechanism of the

- August 7, 1966 El Golfo earthquake, *Bull. Seismol. Soc. Am.*, *68*, 1281-1292, 1978.
- Ekström, G., A very broad band inversion method for the recovery of earthquake source parameters, *Tectonophysics*, *166*, 73-100, 1989.
- Engeln, J. F., D. A. Wiens, and S. Stein, Mechanisms and depths of Atlantic transform earthquakes, *J. Geophys. Res.*, *91*, 548-577, 1986.
- Fornari, D. J., D. G. Gallo, M. H. Edwards, J. A. Madsen, M. R. Perfit, and A. N. Shor, Structure and topography of the Siqueiros transform fault system: Evidence for the development of intra-transform spreading centers, *Mar. Geophys. Res.*, *11*, 263-300, 1989.
- Fox, P. J., and D. G. Gallo, A tectonic model for ridge-transform-ridge plate boundaries: Implications for the structure of oceanic lithosphere, *Tectonophysics*, *104*, 205-242, 1984.
- Fox, P. J., and D. G. Gallo, The geology of North Atlantic transform plate boundaries and their aseismic extensions, in *The Geology of North America*, vol. M, *The Western North Atlantic Region*, edited by P. R. Vogt and B. E. Tuckolke, pp. 157-172, Geological Society of America, Boulder, Colo., 1986.
- Francis, T. J. G., I. T. Porter, and R. C. Lilwall, Microearthquakes near the eastern end of St. Paul's Fracture Zone, *Geophys. J. R. Astron. Soc.*, *53*, 201-217, 1978.
- Froidevaux, C., Energy dissipation and geometric structure at spreading plate boundaries, *Earth Planet. Sci. Lett.*, *20*, 419-424, 1973.
- Futterman, W. I., Dispersive body waves, *J. Geophys. Res.*, *67*, 5279-5291, 1962.
- Gallo, D., P. J. Fox, and K. C. Macdonald, A Sea Beam investigation of the Clipperton transform fault: The morphotectonic expression of a fast-slipping transform boundary, *J. Geophys. Res.*, *91*, 3455-3467, 1986.
- Goff, J. A., E. A. Bergman, and S. C. Solomon, Earthquake source mechanisms and transform fault tectonics in the Gulf of California, *J. Geophys. Res.*, *92*, 10,485-10,510, 1987.
- Harvey, D., and G. L. Choy, Broad-band deconvolution of GDSN data, *Geophys. J. R. Astron. Soc.*, *69*, 659-668, 1982.
- Haxby, W. F., and E. M. Parmentier, Thermal contraction and the state of stress in the oceanic lithosphere, *J. Geophys. Res.*, *93*, 6419-6429, 1988.
- Huang, P. Y., S. C. Solomon, E. A. Bergman, and J. L. Nabelek, Focal depths and mechanisms of Mid-Atlantic Ridge earthquakes from body waveform inversion, *J. Geophys. Res.*, *91*, 579-598, 1986.
- Jones, L., Focal mechanisms and the state of stress on the San Andreas fault in southern California, *J. Geophys. Res.*, *93*, 8869-8891, 1988.
- Jordan, T. H., and K. A. Sverdrup, Teleseismic location techniques and their applications to earthquake clusters in the south-central Pacific, *Bull. Seismol. Soc. Am.*, *71*, 1105-1130, 1981.
- Kawasaki, I., Y. Kawahara, I. Takata, and N. Kosugi, Mode of seismic moment release at transform faults, *Tectonophysics*, *118*, 313-327, 1985.
- King, G., and J. Nabelek, Role of fault bends in the initiation and termination of earthquake rupture, *Science*, *228*, 984-987, 1985.
- Klitgord, K., and J. Mammerickx, Northern East Pacific Rise: Magnetic anomaly and bathymetric framework, *J. Geophys. Res.*, *87*, 6725-6750, 1982.
- Lachenbruch, A. H., and J. H. Sass, Heat flow and energetics of the San Andreas fault zone, *J. Geophys. Res.*, *85*, 6185-6222, 1980.
- Lachenbruch, A. H., and G. A. Thompson, Oceanic ridges and transform faults: Their intersection angles and resistance to plate motion, *Earth Planet. Sci. Lett.*, *15*, 116-122, 1972.
- Laughton, A. S., R. B. Whitmarsh, and M. T. Jones, The evolution of the Gulf of Aden, *Philos. Trans. R. Soc. London, Ser. A.*, *267*, 227-266, 1970.
- Lonsdale, P., Tectonic and magmatic ridges in the Eltanin fault system, south Pacific, *Mar. Geophys. Res.*, *8*, 203-242, 1986.
- Lonsdale, P., Segmentation of the Pacific-Nazca spreading center, 1° N-20° S, *J. Geophys. Res.*, *94*, 12,197-12,225, 1989.
- Lonsdale, P., Structural patterns of the Pacific floor offshore of peninsular California, *AAPG Mem.*, *47*, 87-125, 1991.
- Louden, K. E., R. S. White, C. G. Potts, and D. W. Forsyth, Structure and seismotectonics of the Vema Fracture Zone, Atlantic Ocean, *J. Geol. Soc. London*, *143*, 795-805, 1986.
- Macdonald, K. C., K. Kastens, S. Miller, and F. N. Spiess, Deep-tow studies of the Tamayo transform fault, *Mar. Geophys. Res.*, *4*, 37-70, 1979.
- Macdonald, K. C., D. A. Castillo, S. P. Miller, P. Fox, K.A. Kastens, and E. Bonatti, Deep-tow studies of the Vema Fracture Zone, 1; Tectonics of a major slow slipping transform fault and its intersection with the Mid-Atlantic Ridge, *J. Geophys. Res.*, *91*, 3334-3354, 1986.
- Madsen, J. A., P. J. Fox, and K. C. Macdonald, Morphotectonic fabric of the Orozco transform fault: Results from a Sea Beam investigation, *J. Geophys. Res.*, *91*, 3439-3454, 1986.
- Mammerickx, J., S. M. Smith, I. L. Taylor, and T. E. Chase, Topography of the South Pacific, map, Scripps Inst. Oceanogr., Univ. of Calif., San Diego, La Jolla, 1975.
- Matthews, D. H., The Owen Fracture Zone and the northern end of the Carlsberg Ridge, *Philos. Trans. R. Soc. London, Ser. A*, *259*, 172-197, 1966.
- Mayes, C. L., L. A. Lawver, and D. T. Sandwell, Tectonic history and new isochron chart of the South Pacific, *J. Geophys. Res.*, *95*, 8543-8568, 1990.
- McKenzie, D. P., The relation between fault plane solutions for earthquakes and the directions of the principal stresses, *Bull. Seismol. Soc. Am.*, *59*, 591-601, 1969.
- McNally, K. C., T. Lay, M. Protti-Quesada, G. Valensise, D. Orange, and R. S. Anderson, Santa Cruz Mountains (Loma Prieta) earthquake, *Eos Trans. AGU*, *70*, 1463, 1467, 1989.
- Melson, W. G., S. R. Hart, and G. Thompson, St. Paul's rocks, equatorial Atlantic: Petrogenesis, radiometric ages and implications on sea-floor spreading, *Mem. Geol. Soc. Am.*, *132*, 241-272, 1972.
- Menard, H. W., and T. Atwater, Changes in direction of sea floor spreading, *Nature*, *219*, 463-467, 1968.
- Molnar, P., T. Atwater, J. Mammerickx, and S. M. Smith, Magnetic anomalies, bathymetry and the tectonic evolution of the South Pacific since the late Cretaceous, *Geophys. J. R. Astron. Soc.*, *40*, 383-420, 1975.
- Mount, V. S., and J. Suppe, State of stress near the San Andreas fault: Implications for wrench tectonics, *Geology*, *15*, 1143-1146, 1987.
- Nabelek, J. L., Determination of earthquake source parameters from inversion of body waves, Ph.D. thesis, 346 pp., Mass. Inst. of Technol., Cambridge, 1984.
- Nabelek, J., W.-P. Chen, and H. Ye, The Tangshan earthquake sequence and its implications for the evolution of the North China Basin, *J. Geophys. Res.*, *92*, 12,615-12,628, 1987.
- Ness, G. E., and M. W. Lyle, A seismo-tectonic map of the gulf and peninsular province of the Californias, *AAPG Mem.*, *47*, 71-77, 1991.
- Parmentier, E. M., and W. F. Haxby, Thermal stresses in the oceanic lithosphere: Evidence from geoid anomalies at fracture zones, *J. Geophys. Res.*, *91*, 7193-7204, 1986.
- Parsons, B., and J. G. Sclater, An analysis of the variation of ocean floor bathymetry and heat flow with age, *J. Geophys. Res.*, *82*, 803-827, 1977.
- Phipps Morgan, J., and D. W. Forsyth, Three-dimensional flow and temperature perturbations due to a transform offset: Effects on oceanic crustal and upper mantle structure, *J. Geophys. Res.*, *93*, 2955-2966, 1988.
- Phipps Morgan, J., and E. M. Parmentier, Lithospheric stress near a ridge-transform intersection, *Geophys. Res. Lett.*, *11*, 113-116, 1984.
- Prothero, W. A., and I. D. Reid, Microearthquakes on the East Pacific Rise at 21° N and the Rivera Fracture Zone, *J. Geophys. Res.*, *87*, 8509-8518, 1982.
- Sandwell, D. T., Thermal stress and the spacings of transform faults, *J. Geophys. Res.*, *91*, 6405-6417, 1986.
- Saucier, F. J., E. D. Humphreys, and R. J. Weldon, Stress near geometrically complex strike-slip faults: Application to the San Andreas fault at Cajon Pass, southern California, *J. Geophys. Res.*, *97*, 5081-5094, 1992.
- Schilling, J.-G., B. McCully, and H. Bougault, Mid-Atlantic Ridge volcanism in the equatorial region (3°S-5°N) (abstract), *Eos Trans. AGU*, *68*, 1508, 1987.
- Segall, P., and D. D. Pollard, Mechanics of discontinuous faults, *J. Geophys. Res.*, *85*, 4337-4350, 1980.
- Sibson, R. H., Stopping of earthquake ruptures at dilational fault jogs, *Nature*, *316*, 248-251, 1985.
- Sibson, R. H., Rupture interaction with fault jogs, in *Earthquake Source Mechanics*, *Geophys. Monogr. Ser.*, vol. 37, edited by S. Das, J. Boatwright, and C. H. Scholz, pp. 157-167, AGU, Washington, D. C., 1986.
- Sinton, J. M., Ultramafic inclusions and high-pressure xenocrysts in submarine basanitoid, equatorial Mid-Atlantic Ridge, *Contrib. Mineral. Petrol.*, *70*, 49-57, 1979.

- Stein, C. A., and J. R. Cochran, The transition between Sheba Ridge and Owen Basin: Rifting of old oceanic lithosphere, *Geophys. J. R. Astron. Soc.*, *81*, 47-74, 1985.
- Stein, S., A model for the relation between spreading rate and oblique spreading, *Earth Planet. Sci. Lett.*, *39*, 313-318, 1978.
- Stein, S., and D. A. Wiens, Depth determination for shallow teleseismic earthquakes: Methods and results, *Rev. Geophys.*, *24*, 806-832, 1986.
- Stewart, L. M., and E. A. Okal, Seismicity and aseismic slip along the Eltanin Fracture Zone, *J. Geophys. Res.*, *88*, 10,495-10,507, 1983.
- Stock, J. M., K. M. Marks, and F. R. Schult, Mismatch of fracture zones across the Pacific-Antarctic Ridge (abstract), *Eos Trans. AGU*, *72* (44), Fall Meeting, suppl., 444, 1991.
- Sykes, L. R., Mechanism of earthquakes and nature of faulting on the mid-oceanic ridges, *J. Geophys. Res.*, *72*, 2131-2153, 1967.
- Sylvester, A. G., Strike-slip faults, *Geol. Soc. Am. Bull.*, *100*, 1666-1703, 1988.
- Tréhu, A. M., and G. M. Purdy, Crustal structure in the Orozco transform zone, *J. Geophys. Res.*, *89*, 1834-1842, 1984.
- Tréhu, A. M., and S. C. Solomon, Earthquakes in the Orozco transform zone: Seismicity, source mechanisms, and tectonics, *J. Geophys. Res.*, *88*, 8203-8255, 1983.
- Turcotte, D. L., Are transform faults thermal contraction cracks?, *J. Geophys. Res.*, *79*, 2573-2577, 1974.
- Whitmarsh, R. B., The Owen Basin off the southeast margin of Arabia, *Geophys. J. R. Astron. Soc.*, *58*, 441-470, 1979.
- Wiens, D. A., and D. E. Petroy, The largest recorded earthquake swarm: Intraplate faulting near the Southwest Indian Ridge, *J. Geophys. Res.*, *95*, 4735-4750, 1990.
- Wilcock, W. S. D., G. M. Purdy, and S. C. Solomon, Microearthquake evidence for extension across the Kane transform fault, *J. Geophys. Res.*, *95*, 15,439-15,462, 1990.
- Wilson, J. T., A new class of faults and their bearing on continental drift, *Nature*, *207*, 343-347, 1965.
- Zoback, M. D., et al., New evidence on the state of stress of the San Andreas fault system, *Science*, *238*, 1105-1111, 1987.

E. A. Bergman, U.S. Geological Survey, P.O. Box 25046, Mail Stop 967, Denver Federal Center, Denver, CO 80225.

S. C. Solomon, Department of Terrestrial Magnetism, Carnegie Institution of Washington, 5241 Broad Branch Road, N. W., Washington, DC 20015.

C. J. Wolfe, Department of Earth, Atmospheric, and Planetary Sciences, Room 54-822, Massachusetts Institute of Technology, Cambridge, MA 02139.

(Received March 27, 1992;
revised March 23, 1993;
accepted April 1, 1993.)